

THE CONSTRAINED BLISTER — A NEARLY CONSTANT  
STRAIN ENERGY RELEASE RATE TEST FOR ADHESIVES

by

Yeh-Hung Lai

Thesis submitted to the Faculty of the  
Virginia Polytechnic Institute and State University  
in partial fulfillment of the requirements for the degree of

MASTER OF SCIENCE

in

Engineering Mechanics

APPROVED:

---

D.A. Dillard, Chairman

---

O.H. Griffin

---

S.M. Holzer

December, 1988

Blacksburg, Virginia

THE CONSTRAINED BLISTER — A NEARLY CONSTANT  
STRAIN ENERGY RELEASE RATE TEST FOR ADHESIVES

by

Yeh-Hung Lai

Committee Chairman: D.A. Dillard

Engineering Science and Mechanics

(ABSTRACT)

This study developed and analyzed a modification of the blister test permitting nearly constant strain energy release rate testing of adhesive bonds. The work consisted of three parts; (1) development of the testing technique to evaluate strain energy release rate and to record the time dependent nature of the fracture process, (2) numerical analysis of the constrained blister test to determine the applicability of an approximate solution for several materials, and (3) development of an analytical technique to evaluate the strain energy release rate for relatively stiff specimens.

## ACKNOWLEDGEMENTS

The author wishes to express his acknowledgement for the financial support of Virginia Center for Innovative Technology. He is also deeply indebted to his advisor, Dr. D.A. Dillard who introduced the subject of this thesis to the author. His continual support and assistance aided greatly in completing this work. Also, the author would like to thank two other advisory committee members, Dr. S. M. Holzer and Dr. O. H. Griffin, for their valuable comments on this subject.

Special thanks is extended to \_\_\_\_\_ for his help with most of the experimental work and helpful comments.

Above all, the author wishes to acknowledge the encouragement and the support given by his parents who believe education is the best asset for their children.

## PREFACE

This thesis is composed of three consecutive papers on the subject of a newly developed test called the constrained blister test. Chapter 1 is an introduction and review of the literature. In Chapter 2, an approximate solution is derived: the testing procedure and some typical results of two adhesive tape specimens are also discussed. This chapter is based on a paper written by Y. S. Chang, Dr. D. A. Dillard and the author, which is entitled "The Constrained Blister -- A Nearly Constant Strain Energy Release Rate Test for Adhesives" (accepted, J. of Adhesion). Chapter 3 is based on a paper of numerical analysis for the constrained blister test written by the author and Dr. D. A. Dillard. The paper is entitled "Numerical Analysis of the Constrained Blister Test" (in review, J of Adhesion). Chapter 4 is based on another paper on the subject of the analytical analysis for relatively stiff constrained blister specimens, which is entitled "An Elementary Plate Theory Prediction for Strain Energy Release Rate of the Constrained Blister Test" written by the author and Dr. D. A. Dillard (in review, J of Adhesion). Finally, Chapter 5 is the summary, recommendations, and conclusions of the study. In addition, Appendix A contains some preliminary work on a viscoelastic approach for the case of time dependent membrane adherends.

## TABLE OF CONTENTS

	<u>Page</u>
ABSTRACT .....	ii
ACKNOWLEDGEMENTS .....	iii
PREFACE .....	iv
1. INTRODUCTION .....	1
Figures .....	5
2. TESTING METHODS AND RESULTS .....	6
An Approximate Solution for the Test .....	6
Experimental Setup .....	10
Typical Results for Adhesive Tapes .....	11
Figures .....	16
3. FINITE ELEMENT ANALYSIS .....	23
Results and Discussions .....	25
Figures .....	36
4. THE APPLICATION OF ELEMENTARY PLATE THEORY TO PREDICT STRAIN ENERGY RELEASE RATE .....	47
An Elementary Plate Solution for CBT .....	47
Results and Discussions .....	52
Figures .....	61
5. SUMMARY, RECOMMENDATIONS, AND CONCLUSIONS .....	69
Summary of Work .....	69
Recommendations .....	71

Conclusions .....	72
REFERENCES .....	73
APPENDIX .....	75
Simulation of the Debonding Process for a Strip of Viscoelastic Adhesive Tape .....	75
Results and Discussions .....	80
Figures .....	84
VITA .....	90

## Chapter 1

### Introduction

Over the years, a large number of test geometries have been devised for evaluating the properties of in situ adhesives. The use of fracture mechanics has provided a rational basis for the design of structural components and a number of tests have been developed for measuring these properties. These include such tests as the double cantilever beam (DCB) test originally developed by Mostovoy [1], the cone pull-out test developed by Anderson, et al [2], and the blister test originally employed for paints by Dannenberg [3], and later adapted to structural adhesives by Williams [4]. Each of these tests has certain advantages and disadvantages and each may be modified to provide some degree of mixture between mode I, II, and III crack growth. Among these tests, the blister specimen (Fig. 1-1) offers an attractive alternative for environmental exposure because the diffusion occurs nearly perpendicular to the debond front so that penetration from the sides does not present a problem [5]. Also, because of the axisymmetric nature of the blister specimen, the non-uniformity of the stress field along the debond front is much less than for a finite width specimen. One of the most difficult problems associated with the blister specimen is the determination of the debond radius. Although several techniques have been proposed to identify the increments of crack growth and to detect debond

initiation [6,7], adequate information about actual debond size is still quite difficult to obtain in certain applications.

Measurement of the debond size is important for two reasons -- the determination of the increments in crack growth and the evaluation of the debond radius for calculation of the strain energy release rate. Anderson, et al [7] have discussed closed form and numerical solutions for the strain energy release rate and have identified regions of applicability for formulae for a penny shaped crack between two semi-infinite media and for plate theory. If the deformations are large compared to the blister thickness, the analysis must be further modified to include membrane effects as well [8]. For illustration purposes, we consider the simplest case where thin plate assumptions with small deformations are applicable. The closed form solution is:

$$G = \frac{3 ( 1 - \nu^2 )}{32 E t^3} p^2 a^4 \quad ( 1 )$$

where

G is the strain energy release rate,

$\nu$  is the Poisson's ratio,

E is the Young's modulus,

p is the pressure in the blister,

a is the debond radius, and

t is the thickness of the specimen.

It should be noted that alternate formulations appropriate when the above assumptions are not applicable are given in Refs. 7, 8, and 9. In this simplest case, since radius appears to the fourth power, small errors in measuring the debond will result in significant errors in estimating G.

Another type of blister specimen also of interest to our present purpose is the case of a very thin blister adherend in which membrane stiffness is significantly larger than the bending stiffness. This solution has been given recently by Gent and Lewandowski [8]. They show that the strain energy release rate is given by

$$G = 0.65 p y \quad (2-a)$$

where y is the deflection at the center of the blister and is proportional to

$$y \propto \left[ \frac{p a^4}{E t} \right]^{1/3} \quad (2-b)$$

Although the debond radius is not difficult to obtain for these specimens because of the large displacements, G remains an increasing

function of  $a$ , resulting in non-stable debonding at constant pressure loading. Other relevant geometries were recently proposed by Allen and Senturia for the case of thin films in the blister test of annular and rectangular shapes with and without residual stresses [9, 10]. The current work will neglect residual stresses, a reasonable assumption for the geometries considered.

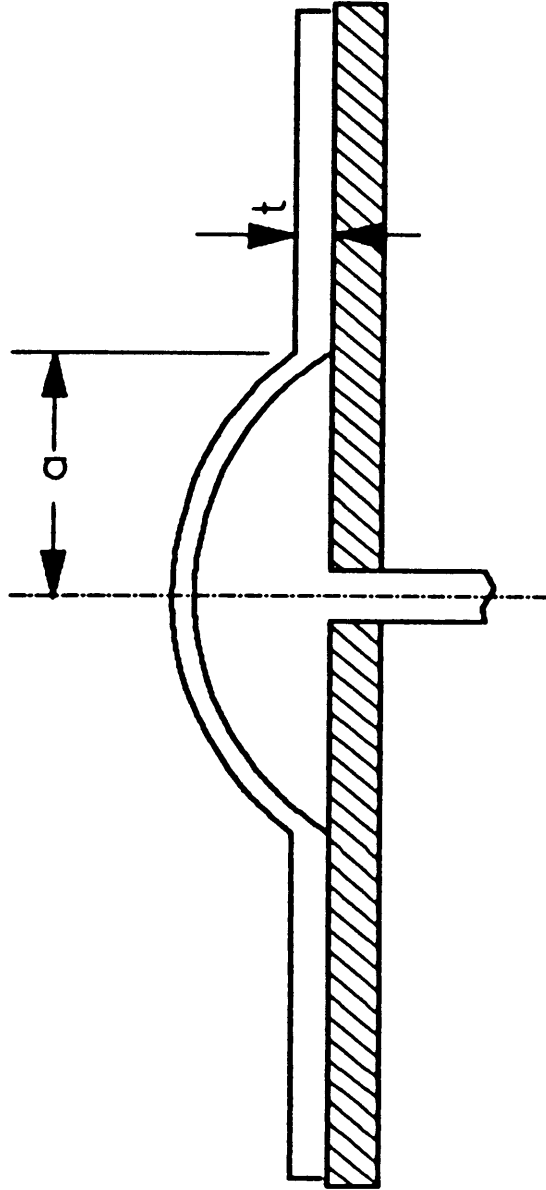


Figure 1.1 Blister test geometry.

## Chapter 2

### TESTING METHODS AND RESULTS

A constant  $G$  test results when the compliance of a specimen increases linearly with crack area, which is the case in the double cantilever beam test. If a flat constraint is placed above the blister to limit its displacement as indicated in Fig. 2.1 and the suspended specimen between the upper constraint and the bottom substrate is vertical then the volume displaced is exactly proportional to the debond area and a constant strain energy release rate test is established. However, the above case is an idealized case; for the realistic case in which the suspended specimen is not vertical, the volume displaced is only approximately proportional to the debond area, which results in a nearly constant strain energy release rate test.

#### An Approximate Solution for the Test

For the geometry indicated in Fig. 2.1, the energy balance as the debond grows may be expressed as:

$$G_c \delta A = \delta W - \delta U - \delta Z \quad (3)$$

where

$G_c$  is the critical value of strain energy release rate

and may be a function of debond rate and environment,  
 $\delta A$  is the variation of the debond area,  
 $\delta W$  is the variation in work done on the system,  
 $\delta U$  is the variation of the strain energy of the specimen, and  
 $\delta Z$  is the variation of the energy dissipated in region  
 away from the vicinity of the debond tip, which may  
 include viscoelastic, frictional effects and plastic  
 dissipation.

The energy balance formalism used here is based on the classical energy conservation approach where localized viscoelastic and plastic deformations in the vicinity of the crack tip are included in the strain energy release rate,  $G_c = G_c(da/dt)$ , making it a function of debond rate. The choice to include this near field energy dissipation in the  $G_c$  term provides expediency, and has been discussed by Knauss [11] Williams [12], and used by Anderson, et al. [7] and others [13,14]. This is a reasonable approach since near field dissipation cannot readily be separated from an "inherent" surface energy anyway.

For non-linear traction-displacement systems, if the relation between the traction and displacement can be expressed as

$$p = (V/C)^n \quad (4)$$

where  $p$  is the generalized traction,

$V$  is the generalized displacement

$C$  is the compliance

and  $n$  is an experimental or analytical constant,  
the strain energy release rate can easily be shown as:

$$G = \frac{n}{n+1} p^{((n+1)/n)} \frac{\partial C}{\partial A} \quad ( 5 )$$

For  $n=3$ ,  $G$  is proportional to  $p^{4/3}$ . Typical examples are the cases for membrane analysis of blister test [8] which is shown in Eqs. (2-a) and (2-b) and the analysis of pull-off force for adhesive tapes [15]. For  $n=1$ , the well known equation for linear system is obtained, and a typical example is the plate theory in Eq. (1). It can also be shown that the stored energy for the general form is only  $1/(n+1)$  of the input work under constant traction cases. As  $n$  increases, the stored energy becomes negligible in comparison to the external work. Figure 2.2 illustrates the pressure-displacement relations for the linear case (which corresponds to plate theory), the cubic case (which corresponds to Gent's membrane analysis [8]), and actual and idealized cases for the constrained blister.

Since the exponent in Eqs. 4, 5 for the case of the constrained blister is often quite large, it leads to the assumption that the variation in stored energy in Eq. 3 is negligible, which will also be demonstrated later from the numerical and analytical analyses. The  $\delta Z$  term is also neglected by assuming that there is little far field viscoelastic dissipation in the blister adherend. We will also neglect energy dissipated at the interface between the blister and the

constraint. This effectively implies that there is no slipping between the blister and the constraint, or that the interface is perfectly lubricated. Experimental and numerical observations tend to support the validity of the former assumption. The above claims allow one to write

$$G_c \delta A \approx \delta W = p \delta V \quad (6)$$

where  $p$  is the applied pressure and  $\delta V$  is the variation in volume under the blister.

To approximate this variation in volume, it is assumed in this chapter that the suspended region of the blister is linear. While this assumption is not consistent with the bending of the blister adherend, it is used only to calculate the volume under this small suspended region and not to obtain bending energy. It will be shown in the numerical analysis chapter that this choice gives an accurate value for the volume under the blister and does not introduce errors elsewhere. Under this linear suspended region assumption, the volume under the blister is given as:

$$V = \pi h \left( a^2 - ad + \frac{d^2}{3} \right) \quad (7)$$

Taking the variation of the volume and substituting into Eq. (6), we obtain that the strain energy release rate is simply the product of the pressure,  $p$ , the constraint height,  $h$ , and a correction factor,  $q$ .

$$G_c = p h q \quad (8)$$

For the case of the linear detachment assumption,  $q$  is given by:

$$q = \left(1 - \frac{d}{2a}\right) + \left(\frac{d}{3a} - \frac{1}{2}\right) \frac{\partial d}{\partial a} \quad (9)$$

Since the detachment distance,  $d$ , changes only slightly as the debond grows, the partial derivative appears to be quite negligible for the cases examined so far.

### Experimental Setup

The test setup designed to test the debonding of adhesive tapes is shown in Fig. 2.3 . The substrate and constraint were made of polycarbonate, facilitating visual observation. To prepare a specimen, the substrate was cleaned and dried at room temperature, and the tape, with a nominal width of 150mm was applied and rubbed to ensure attachment. The substrate had a hole in the center with a diameter of 6 mm. A spacer of the desired thickness was placed above the blister, and the constraint was bolted in place. The pressurizing medium was supplied at constant pressure. For the present case, the pressurizing media was supplied from a large reservoir. The method used to measure the debonding radius, the length of the suspended region and the debonding rate was visual measurement of the debonding diameter and the contact diameter. The length of the suspended region was calculated by subtraction of the respective radii. The change of the blister volume had also been monitored by measuring the volume change in the upper chamber by using a precision syringe and an LVDT. To get

a large window of  $G$  values from one test, one might increase or decrease the pressure several times. To examine the reproducibility of this technique, several specimens were tested to obtain the average debond rates for each pressure. Since the debond radius and suspended distance were recorded for each measurement, the correction factors could easily be calculated according to Eq. 9. This approach provided the most accurate estimates of applied strain energy release rate, but did require a transparent constraint and easily observed debond radii.

#### Typical results for Adhesive Tapes

Two adhesive tapes were used in this study and were supplied by the 3M corporation. Their properties are summarized as follows:

Tape	Backing	Adhesive	Thickness	Modulus (MPa)
A	Polyester	Rubber	0.107 mm	743
B	Vinyl	Acrylic	0.18 mm	7.93

Cross head rate = 25.4 mm/min

It should be noted that tape A behaves like an elastic material, while the properties of tape B are significantly time-dependent. Creep test results are shown in Fig. 2.4 for a strip of tape B. The substrate was polycarbonate which was cleaned with alcohol and dried at room temperature between each use. Distilled water was used as the pressurizing medium. The large width of the tape required special care for uniform application onto the substrate.

A small blister formed as soon as the reservoir valve was opened. Recording of experimental readings commenced when the blister touched the constraint. Data could have been collected prior to contact and used in conjunction with Gent's approach [8]. Each experiment was stopped when the constrained blister reached the edge of the spacer during testing. The adhesive tape was stretched in one direction slightly as it was applied to minimize the formation of wrinkles in the tape. Although the blister started out circular, there was a slight tendency for the blister to grow fastest in the stretch direction, since the membrane stresses were larger in this direction. The deviation from a circular shape was only on the order of 5%, and was not believed to be significant. It is interesting to note that because the pressure acts through nearly the same increment in volume regardless of where the increment of area occurs, debonding in any direction is almost equally likely to occur. This implies that the impetus for symmetry, which is clearly seen in unconstrained blister tests, is significantly reduced with this nearly constant G test. For stronger adhesives, this behavior could result in rather arbitrary debond patterns which could introduce errors into the technique.

Several typical results for the adhesive tapes A and B are shown in Figs. 2.5 to 2.7.

Figure 2.5 illustrates the debond rate, debond radius and

suspended distance for a tape A specimen using a spacer thickness of 3.175 mm and a constant pressure ( $p = 28.3$  kPa.). The debonding radius increases linearly with time and the suspended distance decreases only 10% during the same time period. Since  $a$  and  $d$  were measured, the correction factor could be calculated and is about 0.63 when the blister first touched the constraint. Similarly, the correction factor is about 0.80 at the end of the test. Thus the difference of the applied  $G$  is 17%. Despite this small increase in  $G$ , there does not seem to be any significant change in debond rate.

To better understand the effect of  $G$  on debonding rate, a graph with a larger range of  $G$  and debonding rate was constructed for tape A by testing one specimen under several different reservoir heights. Multiple tests were conducted to obtain the average values. To examine the validity of the constrained blister test (CBT), the free membrane blister test (BT) was constructed by measuring the blister height and radius. A series of  $G$  values were obtained by employing Eq. (2), and the corresponding debonding rates were also calculated. Several standard peel tests with different take off angles were also conducted to verify the results. The results of all three techniques, within the range observed on the blister tests, are in good agreement with each other and are shown in Fig. 2.6. The fracture mode in each case was a mixture of mode I and II, but no attempt was made to separate these components.

Figure 2.7 illustrates the testing results for the tape B which is flexible and quite time-dependent. In addition to measuring the debond radius and suspended distance, tape B was also tested by monitoring the volume displacement, and thus, the debond area was obtained. It is seen that the suspended distance is small, even at the beginning of the test. The approximate  $q$  value at this stage is about 0.92 and increased to 0.98. Thus the variation of  $G$  values for these tests under constant pressure is only about 6%, which is smaller than that of the stiffer tape A. Based on the results from tape A, one would expect that the debond rate would be constant for tape B under a constant pressure level. Instead, according to the experimental results, the area debond rate ( $dA/dt$ ) is essentially constant. This implies the radial debond rate decreases as the debond grows. It is believed that this anomalous behavior arises because of the viscoelastic dissipation in tape B. This term was not included in the energy balance, but would not be negligible for this tape material.

An important advantage of the constrained blister test is that desired  $G$  values can be obtained by any combination of  $p$  and  $h$ , as indicated by Eq. (8). Using two spacer thicknesses 3.2 mm. (0.125 in) and 5.6 mm. (0.219 in)) and holding at constant pressures selected to achieve equivalent strain energy release rates of  $98 \text{ J/m}^2$ , the debond rates are constant with time and superpose very well as seen in Fig. 10. Thus one can select a pressure and constraint height combination to achieve the desired strain energy release rate. In practice it is

preferable to keep the height as small as possible to minimize the need for the correction. In doing so, however, one must not allow the pressures to become so high that they rupture the blister. As suggested by Napolitano, et al [16], however, the constraint significantly reduces the membrane stresses and allow testing at pressures much higher than would be possible with a free membrane.

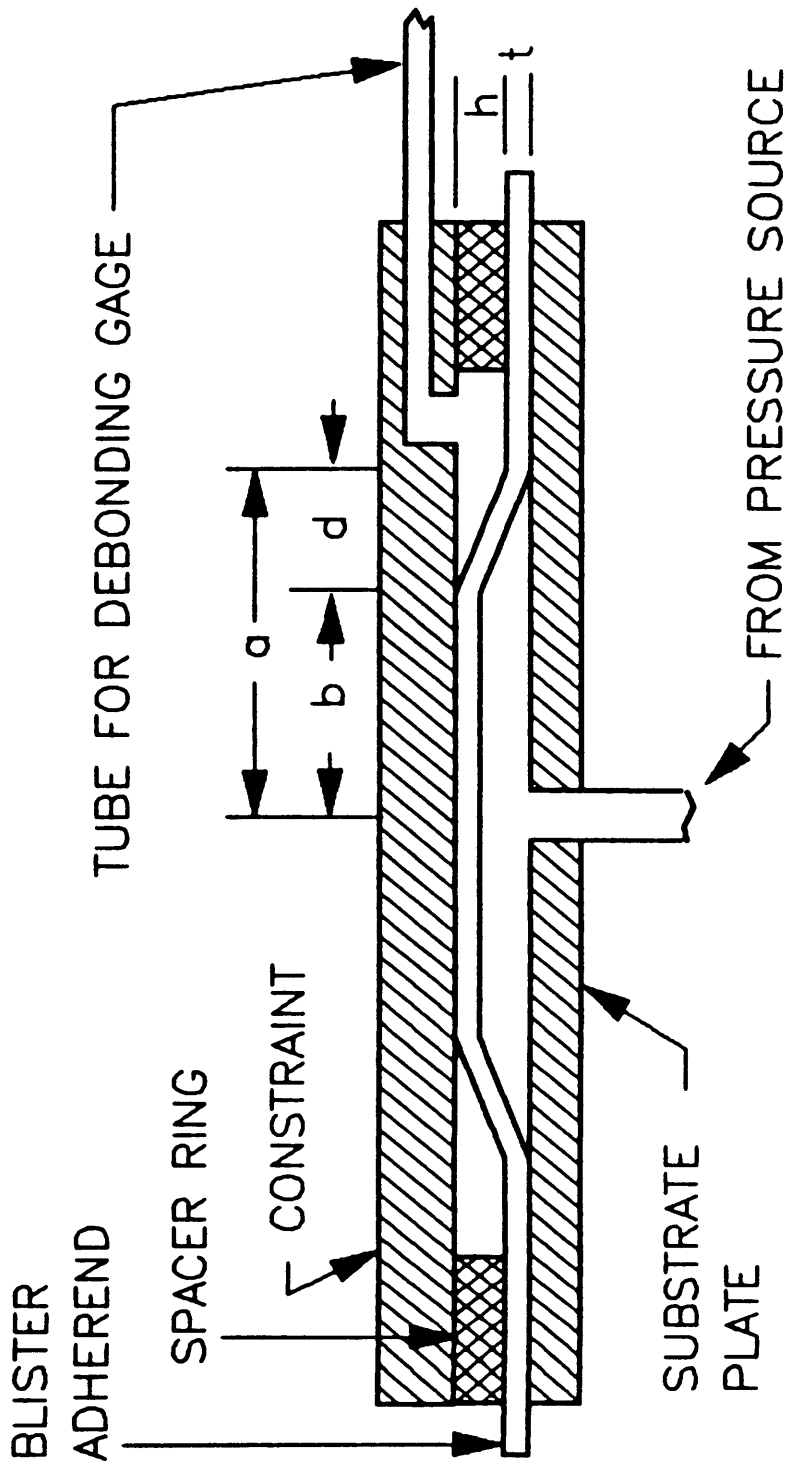


Figure 2.1 Constrained blister test geometry.

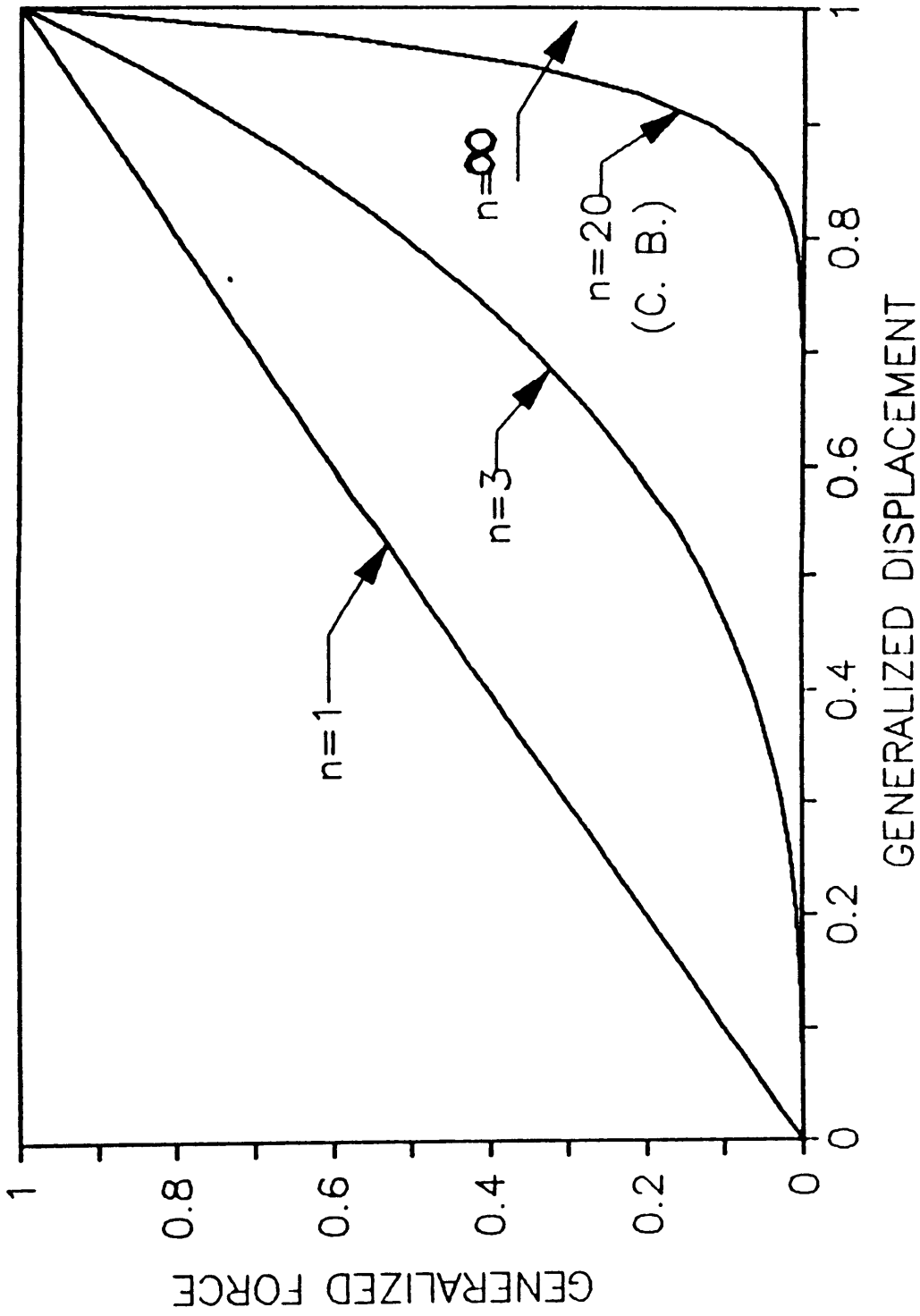


Figure 2.2 Nonlinear force - displacement curves.

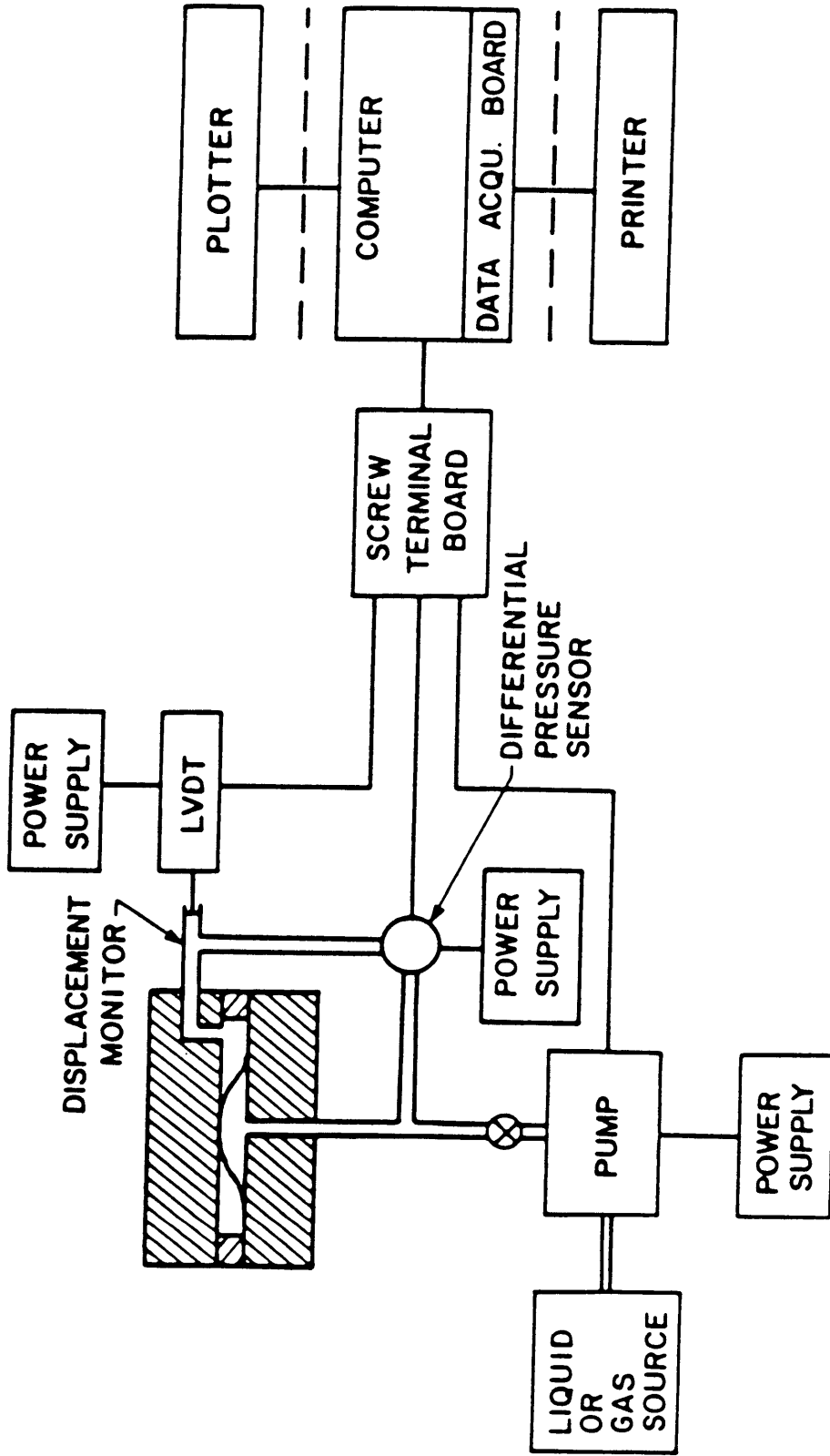


Figure 2.3 The experimental setup for the constrained blister test.

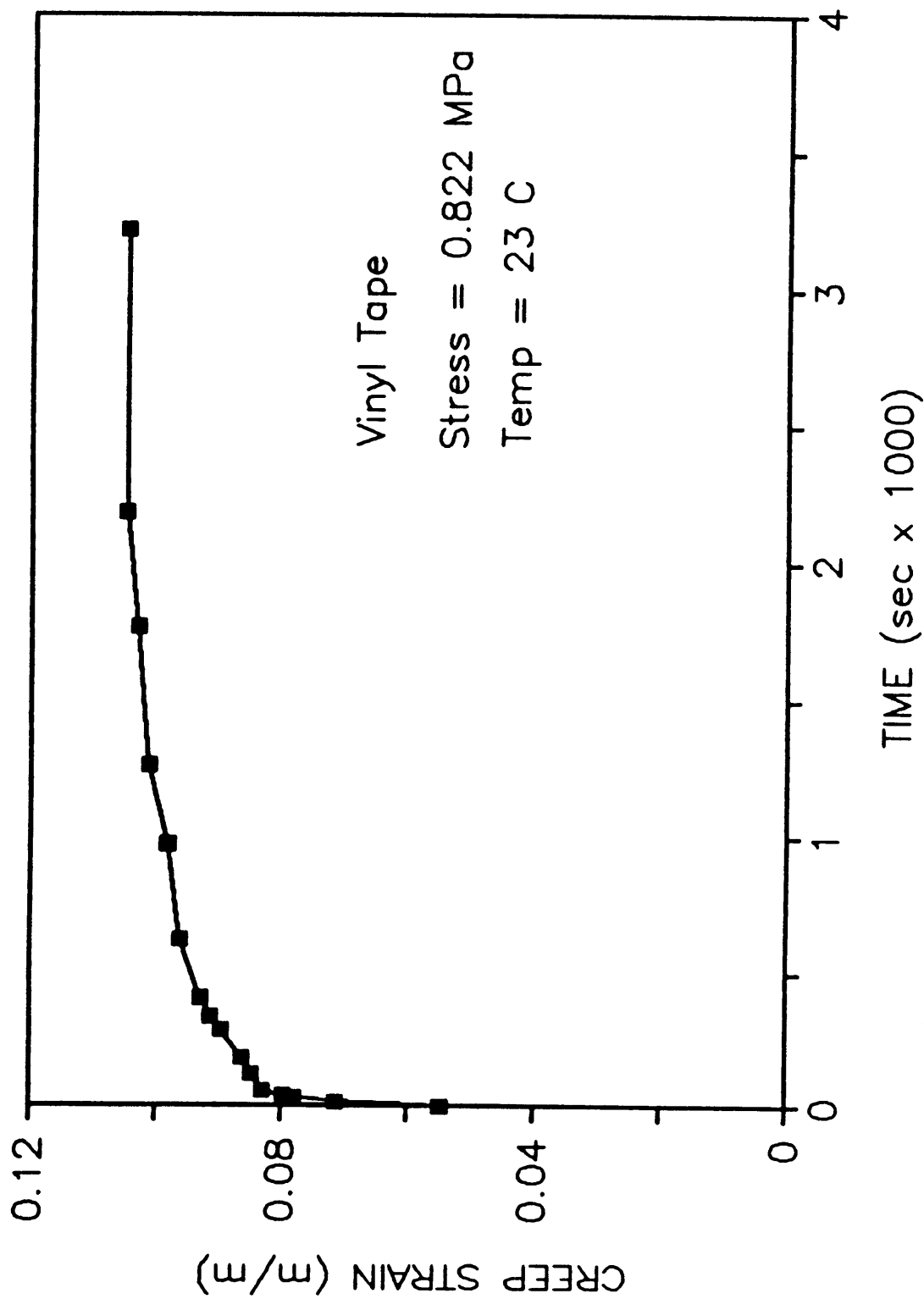


Figure 2.4 Creep test results for the vinyl tape.

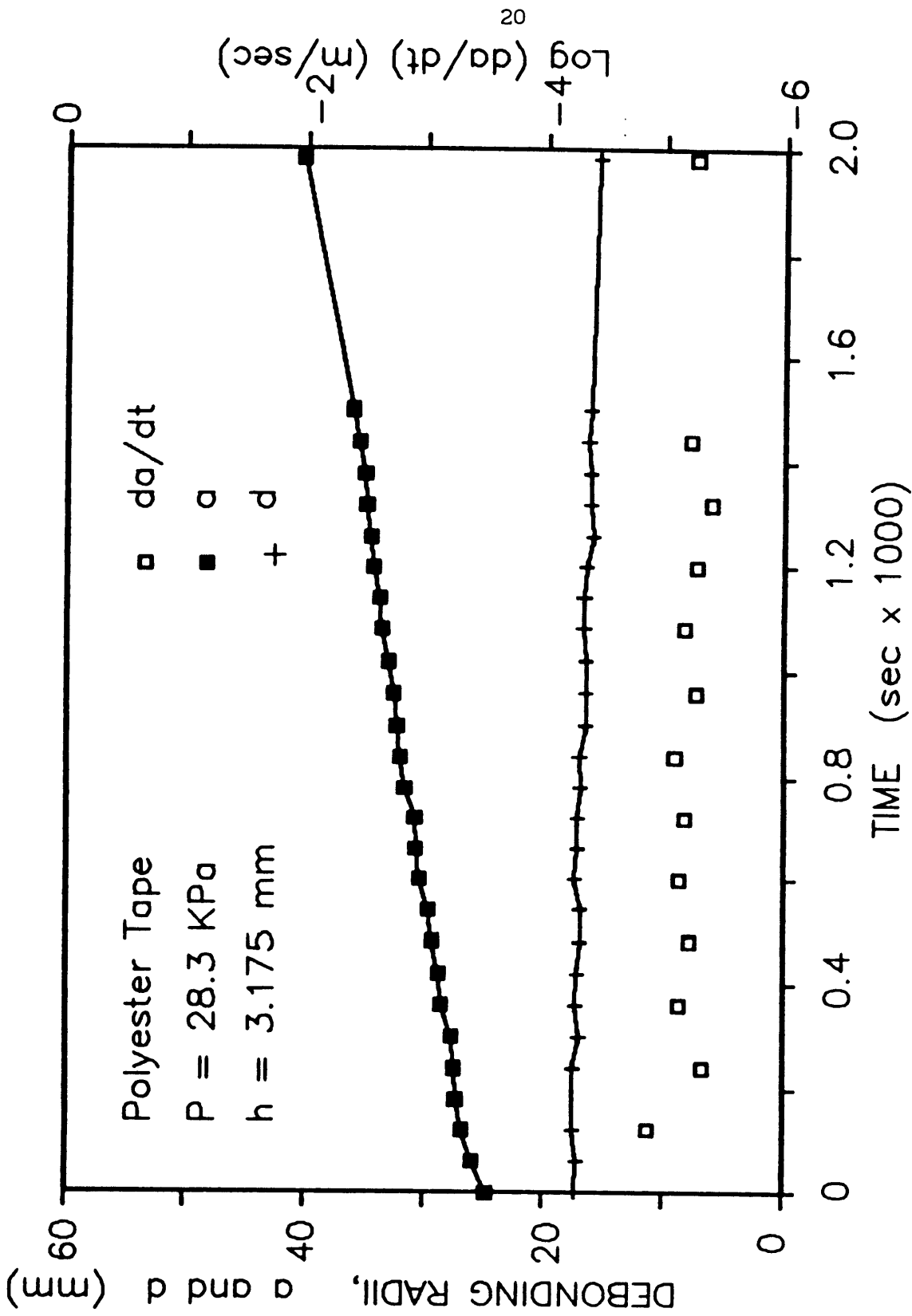


Figure 2.5 Debonding results for a polyester tape.

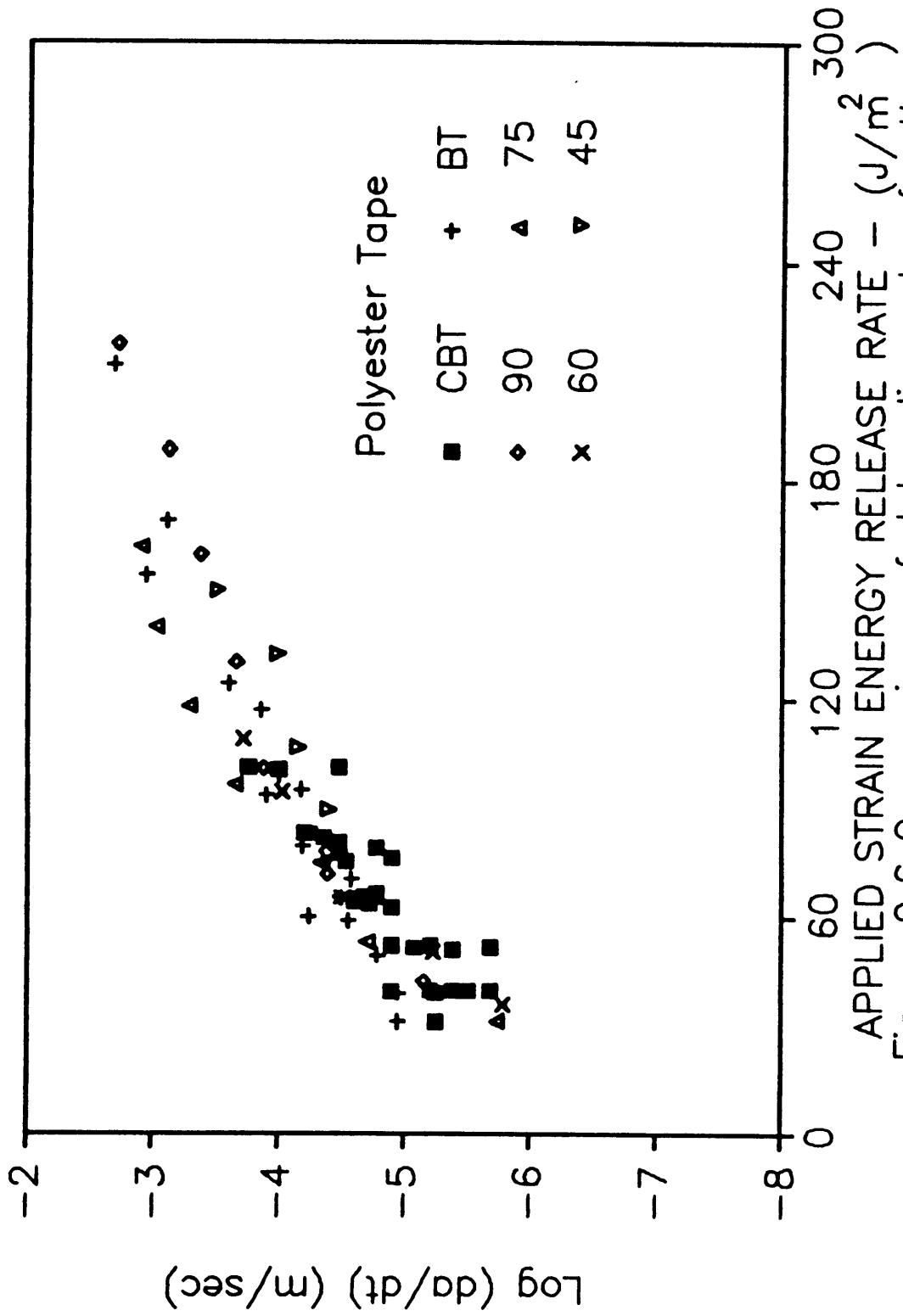


Figure 2.6 Comparison of debonding rates for the CBT, BT and Peel Test.

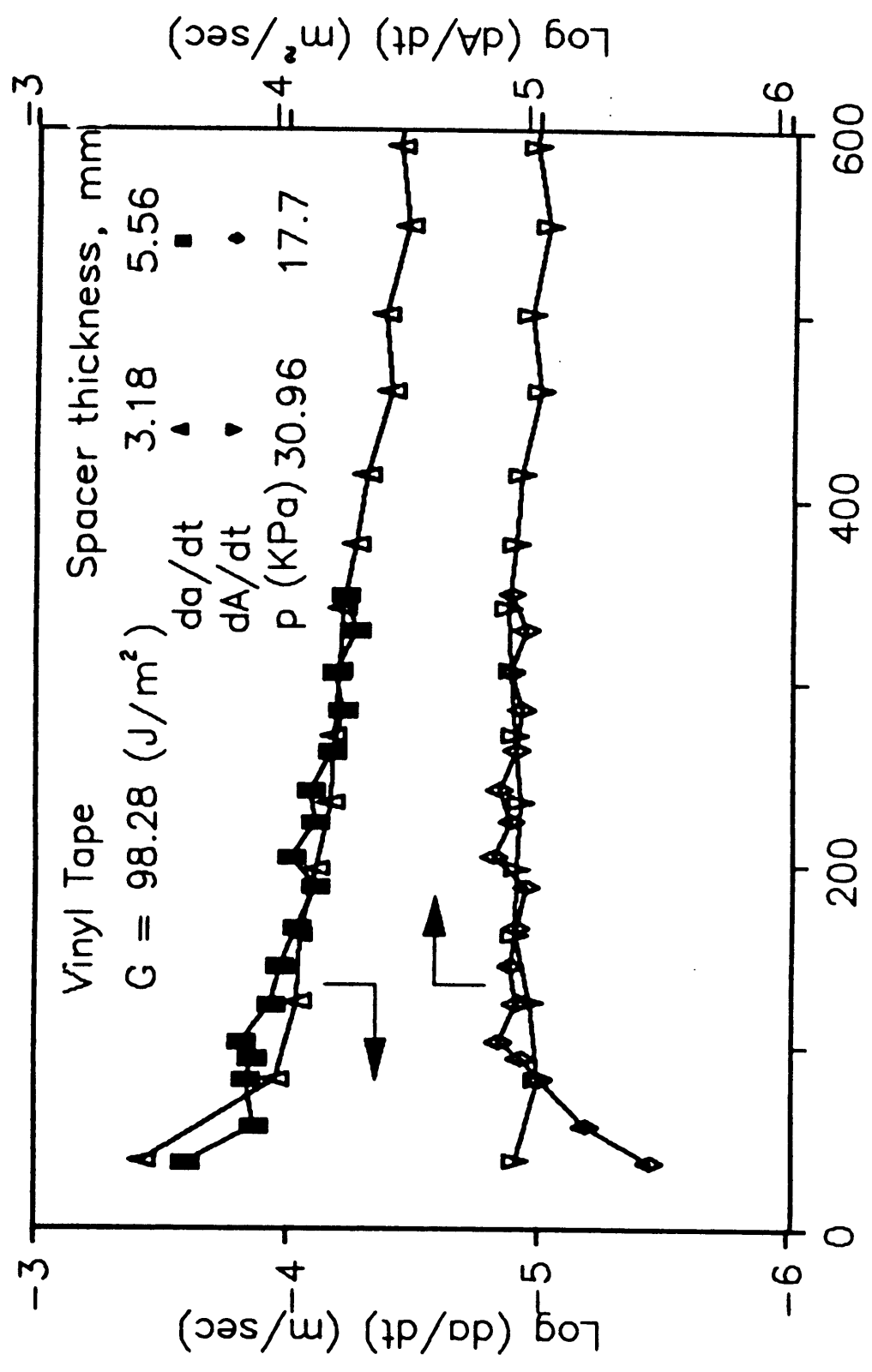


Figure 2.7 Debonding results for a vinyl tape.

## Chapter 3

### FINITE ELEMENT ANALYSIS

In order to model the contact between the blister and the upper constraint, a finite element program called ABAQUS was used because of its capabilities to handle contact problems. Since the geometry and boundary conditions were axisymmetric, an axisymmetric, biquadratic element was used. All the materials analyzed were assumed to be linearly elastic. Thus, although the fracture process within the adhesive might involve considerable localized viscoelastic dissipation, gross viscoelastic effect away from the fracture zone were not considered. ABAQUS had been used to analyze several adhesive system and geometry configuration. Only two cases are reported herein: 1) an aluminum blister and 2) a tape blister. One of the typical deformed meshes and the refined mesh near the crack front of an aluminum specimen are shown in Fig. 3.1. For the present analysis, no element were used to model the adhesive layer itself, although this could be done for greater accuracy.

Although ABAQUS has nonlinear geometry capabilities, convergence could not be obtained for all cases analyzed. In this study, only the aluminum cases were analyzed with the geometrically nonlinear option, while the adhesive tape case were analyzed with the linear option. Although the nonlinear analysis gives a significantly different mode

mix than the linear analyses, the total strain energy release rates were almost identical for the aluminum case.

Version 4-5-154 of ABAQUS provided good results using the J-integral evaluation option for the standard blister test. However, unrealistic J-integral and strain energy values of several times higher than applied work were obtained when the specimen contacted the upper constraint. To avoid these errors in the ABAQUS program, equations of energy release rates for an interfacial crack by Smelser [17,18] were applied to the crack between the rigid substrate and elastic blister adherend. The equations for strain energy release rates are as follows:

$$G_T = \frac{\pi \mu \lambda_0^2}{2(1-\nu)} \frac{u^2 + v^2}{r} \quad (10-a)$$

$$G_I = \frac{\pi \mu \lambda_0^2}{2(1-\nu)} \frac{v^2}{r} \quad (10-b)$$

$$G_{II} = \frac{\pi \mu \lambda_0^2}{2(1-\nu)} \frac{u^2}{r} \quad (10-c)$$

where

$G_T$  is the total strain energy release rate,

$G_I$  is the mode I strain energy release rate,

$G_{II}$  is the mode II strain energy release rate,

$u$  is the tangential crack opening displacement at a point near the crack front,

$v$  is the normal crack opening displacement at a point near the crack front,

$\mu$  is the shear modulus of the specimen,

$r$  is the distance from the crack front,

$$\epsilon = \frac{1}{2\pi} \ln ( 3 - 4 \nu ) ,$$

$$\lambda_0 = \frac{1}{2} ( 1 + 4 \epsilon^2 ) ,$$

and  $\nu$  is the Poisson's ratio of the specimen.

### Results and Discussions

In order to verify the applicability of Eq. (8) for the constrained blister test, typical cases were analyzed with different parameters. Figures 3.2-3.6 are the cases for 6061-T6 aluminum specimens which have a Young's modulus of 68.93 GPa and Poisson's ratio of 0.3. Figures 3.7-3.10 are the cases for typical adhesive tapes. In these cases, the Young's modulus is 150 MPa and Poisson's ratio is 0.44. Figure 3.2 illustrates the typical stress distributions obtained by a geometrically nonlinear analysis at the lower side of an aluminum specimen which has a thickness of 3 mm, a constraint height of 2 mm and is subjected to a pressure of 200 kPa. The legends denoted ' $\sigma_r$ ', ' $\sigma_\theta$ ' and ' $\sigma_z$ ' stand for the stresses in the radial, circumferential,

and axial directions, respectively. This convention will be used throughout the following figures. Starting from  $r=0$ , a uniform stress distribution is seen in the area that contacts the upper constraint. In the suspended region,  $\sigma_r$  and  $\sigma_\theta$  change signs twice because of the sigmoidal bending, and finally, singularity of  $\sigma_r$  is seen at the crack front. The stress in the  $z$  direction, which has the same magnitude as the applied pressure, is very small compared to the other two stress components so that it is hardly visible in the figure.

Figure 3.3 illustrates the typical stress distributions obtained by nonlinear analyses at the the mid-plane of the same aluminum specimen as in Fig. 3.2. It is seen that membrane stretching stresses,  $\sigma_r$  and  $\sigma_\theta$ , obtained from the nonlinear analysis, remain at the same magnitude within the contacted region but split and decrease near  $r=a$ , while  $\sigma_r$  obtained from linear analysis is quite small and almost constant throughout the whole region. The small drop of  $\sigma_z$  at the inner end of the suspended region indicates the effect of the compressive reaction force from the upper constraint in this local region. It is found that the stretching stresses from the nonlinear analysis in the contacted region are roughly equal to

$$\sigma_\theta \approx \sigma_r \approx \frac{E}{(1-\nu)} \bar{\epsilon}_r$$

where

$\bar{\epsilon}_r$  is the average strain in the r-direction.

This is the expected value. By examining the total deformed length from the nonlinear analysis, good agreement is found by integrating the midplane strains in the radial direction and summing the total lengths of the deformed elements. This suggests that the geometrically nonlinear analysis for the contact problem is reliable for this case.

Figure 3.4 shows the deformed profiles of the aluminum specimen for both linear and nonlinear analyses. It should be noted that the y-axis is greatly enlarged. The displacement in the nonlinear analysis is slightly lower than that in linear analysis in the suspended region and the magnitudes of the length of suspended region are similar in both analyses. It is seen that the suspended region is not a straight line. Since the correction factor,  $q$ , is based on the assumption of linear suspended region, this nonlinearity could induce error when calculating the strain energy release rate from Eq. (8). However, by examining the difference of the volume, the error of strain energy release rate due to this approximation is only about 0.5%.

Figures 3.5-3.10 give strain energy release information for both the aluminum and adhesive tape cases. The legend denoted ' $G=phq$ ' represents the strain energy release rates which are evaluated from Eq. (8). It is noted that when calculating  $q$  using Eq. (9), the length of suspended region,  $d$ , is not calculated from analytical

expressions, but from the finite element results. It is assumed that similar values for  $d$  would have been observed experimentally; furthermore, small errors in  $d$  do not significantly affect the values of strain energy release rate. The legends, 'FEM- $G_T$ ', 'FEM- $G_I$ ' and 'FEM- $G_{II}$ ', stand for the curves which are obtained by using the finite element displacements in Eq. (10-a), (10-b) and (10-c) for total, mode I and mode II strain energy release rates, respectively. Due to the nature of the symmetric geometry, mode III strain energy release rate does not exist. The legend 'G=ph' stands for the strain energy release rate in the limiting case when  $q = 1$ , which corresponds to  $\frac{d}{a} = 0$ . This approximation is seen to be substantially in error for most cases considered.

Figure 3.5 illustrates the strain energy release rates versus debond radius for the case of an aluminum specimen which has the same dimensions and material properties as those in the previous figures.  $G_I$  and  $G_{II}$  obtained from linear analysis are also included for comparison with those obtained from nonlinear analysis and are denoted as " $G_I$ -linear" and " $G_{II}$ -linear", respectively. The rest of the curves are based on the nonlinear analysis. Good agreement for total strain energy release rate is seen between the analytical solution and the nonlinear FEM results. The gap between the curves denoted " $G=phq$ " and " $G=ph$ " shows the necessity for the correction factor,  $q$ . It should be noted that  $q$  is obtained from Eq. (9) by neglecting  $\frac{\partial d}{\partial a}$ . Justification of this assumption is based on experimental observations in Chapter 2

and is also demonstrated numerically in a following section. By comparing  $G_I$  and  $G_{II}$  obtained by linear and nonlinear analyses, it is found that  $G_I$  from the linear analysis is greater than that from the nonlinear analysis, while  $G_{II}$  is smaller. Furthermore, it is seen that the differences between  $G_I$ 's and  $G_{II}$ 's are approximately equal and of opposite signs, thus the total strain energy release rates differ only slightly in the two analyses. Since the difference is less than 0.5%, the total  $G$  from the linear analysis has not been shown in the figure. Although the linear analysis results in substantial mode mix errors, the total  $G$  values appear to be accurate for all cases investigated.

One concern in developing Eq. 8 from Eq. 6 was whether the blister region in contact with the constraint would slip as the blister grows, thereby dissipating a portion of the input work. By changing coefficients of friction from 0.0 to 1.0 for the ABAQUS contact elements, it is found that only a negligible change ( $< 0.01\%$ ) in the strain energy release rate occurs, which shows that neglecting the frictional dissipation is reasonable in deriving Eq. (8).

Figure 3.6 shows the effect of the debond radius on the correction factor and the length of the suspended region. It shows that  $d$  remains nearly constant as  $a$  increases. Therefore, the assumption of neglecting  $\frac{\partial d}{\partial a}$  is reasonable and  $q$  is primarily influenced by  $a$  only. It is seen that  $q$  is smaller than 0.75, thus, the error between the equations,  $G=ph$  and  $G=phq$ , would be greater than 25% and it is

important to determine  $q$  accurately. However, it should be noted that since  $a$  and  $d$  are to the first order in Eq. (9), the error of  $q$  and consequently, error of  $G$ , resulting from a measuring error in  $a$  or  $d$  would be quite small. In the analysis of the aluminum specimens, the total strain energy release rates considered were in the range of 210-320 J/m<sup>2</sup> and the maximum principal stress is 240 MPa in the region away from the singularity point. This is lower than a typical aluminum yielding stress, 275 MPa. The plastic zone is found to be within 0.05% of the thickness, which suggests that the plastic dissipation is negligible. For an adhesive system with adhesive fracture energy higher than 320 J/m<sup>2</sup>, one can either increase pressure or increase constraint height to study debond. It should be noted, however, that higher pressure or constraint height could induce yielding in the blister adherend and thus, induce a large error for the strain energy release rate. In the analysis of this aluminum specimen case, it is also seen that for a small debond radius ( $a < 120$  mm), the specimen would not touch the upper constraint. This indicates that one usually needs specimens with large debond radius and equipment to perform the test on aluminum adherends. Special reinforcement of the constraint may be required to minimize its deflection.

Due to convergence problems encountered in analyzing the following cases of adhesive tapes, only geometrically linear analyses were performed. However, for a thin and soft specimen, such as an adhesive tape, the magnitudes of the stretching membrane stresses are the major

differences between the linear and nonlinear analyses. For an adhesive tape, the  $\sigma_\theta$  stress distribution curve along the radial direction is expected to be closer to  $\sigma_r$  curve than that in Fig. 3.3 for an aluminum specimen and  $\sigma_r$ ,  $\sigma_\theta$ ,  $\epsilon_r$  and  $\epsilon_\theta$  would be nearly uniformly distributed in the whole blister. If one can assume the applied pressure is much smaller than stretching stresses, which is the case in the following analyses, then average stretching strains could be approximated as follows:

$$\epsilon_r = \epsilon_\theta = \frac{(d^2 + h^2)^{1/2} - d}{a}$$

and the stresses as:

$$\sigma_r = \sigma_\theta = \frac{E}{(1-\nu)} \frac{(d^2 + h^2)^{1/2} - d}{a}$$

After obtaining stresses and strains, it can be shown that the variation of strain energy with respect to debond radius due to stretching is:

$$\frac{\partial U}{\partial a} = \frac{\pi}{2} t \left[ 4d - \frac{4d^2 + 2h^2}{(d^2 + h^2)^{1/2}} \right] \frac{E}{(1-\nu)} \frac{\partial d}{\partial a}$$

Thus, since  $d$  is nearly constant as the debond grows, which is true in

most cases examined, the variation of strain energy due to stretching would be negligible compared to the variation of work done in the system and the results of linear analysis would be close to that of nonlinear analysis.

Figure 3.7 illustrates the relationship between the energy release rates and debond radius for the tape specimen with an  $h$  of 3.175 mm and  $t$  of 0.18 mm, corresponding to one layer of adhesive tape B in the previous tests in Chapter 2. The applied pressure is 100 kPa. Good agreement is seen between Eq. (8) predictions and the FEM results. It is found that  $d$  remains nearly constant with a magnitude of 3.7 mm. Although  $q$  in this analysis is smaller than 0.9, it should be noted that as debond radius increases,  $q$  increases. For example, if  $a$  is as large as 50 mm,  $q$  would be around 0.96, which suggests that the effect of  $d$  on  $q$  would be much less significant for large values of  $a$ .

From Figs. 3.5, 3.6, and 3.7, it is seen that as  $a$  becomes larger, the gradient of  $q$  and thus, the rate of increase in  $G$  with respect to  $a$ , becomes smaller. Since  $p$  and  $h$  are held constant, if  $a$  is large enough, energy release rates would be nearly constant; i.e., the test would be a nearly constant strain energy release rate test. The difference between the correction factor and unity, however, may not be negligible.

Figures 3.8 and 3.9 illustrate the strain energy release rates

versus pressure,  $p$ , and constraint height,  $h$ , respectively. The specimen is one layer of adhesive tape with an  $a$  of 8.22 mm. Good agreement is seen between Eq. (8) predictions and FEM results. Approximate linearity is seen between  $G$  and  $p$  and  $G$  and  $h$ .

Figure 3.10 shows the variation of strain energy release rate with respect to various thicknesses of the adhesive tapes. In general, the deviation of the approximate solution (Eq. 8) from FEM results increases as  $t$  increases, which shows that the effect of bending energy plays an increasingly important role in the system as thickness increases. However, when the blister has more than 3 tape layers, the deviation becomes stable and is around 8%. It is noted that for an adhesive tape six layers thick under the same  $p$  and  $a$ , the blister does not contact the upper constraint and the strain energy release rate is approximated by Eq. (1). A large deviation with respect to Eq. (8) is expected.

The previous study of the standard blister test discussed by Anderson et al [7] shows that the loading mode in the blister test specimens changes from near mode I to a combination of mode I and II as the debond radius increases. The ratio of mode I with respect to mode II for various debond radii in the constrained blister test for the cases of thin and thick adhesive tapes and the aluminum specimen is shown in Fig. 3.11. Thicknesses of 0.18 mm for thin adhesive tapes and 3 mm for thick adhesive tapes were used for this figure. The

aluminum specimen is the same as that in Fig. 3.5. The results of linear and nonlinear analyses for the aluminum case are both included in this figure for comparison. In all cases, the ratios remain nearly constant, however, it should be noted that during this thickness-to-diameter range, the free blister has also nearly constant mode ratio. By comparing between the cases of thick adhesive tape and aluminum which have the same dimensions and applied load but different material properties, it is found that mode I is greater than mode II for the thick adhesive tape case, while mode II dominates the debond in the case of aluminum specimen. This phenomenon may be explained because in the former case, the material is softer and the suspended region of the blister is steeper. Thus the stretching stresses in this region result in larger peel forces at the crack front to peel the specimen from the bond line. For the latter case, the material is stiffer, the suspended region of the blister is flatter, and the stretching force in this region results in a larger shear force at the crack front than peel force. The same reason can be used to explain the differences between thin and thick tapes: for the thin adhesive tape case, the constraint height is higher, the debond radius is smaller and applied pressure is lower than those for the thick adhesive tape case, thus, it is expected that the suspended region would be flatter and the ratio between mode I and mode II would be smaller. Consequently, it is expected that in the constrained blister test, mode I would dominate the debond for soft, thin materials subjected to high pressure and high constraint height, and mode II

would dominate for stiff, thick material subjected to low pressure and low constraint height. Although a complete analytical solution is not available, this preliminary study suggests that the loading mode for the constrained blister test depends on the thickness, constraint height, material properties and applied load.

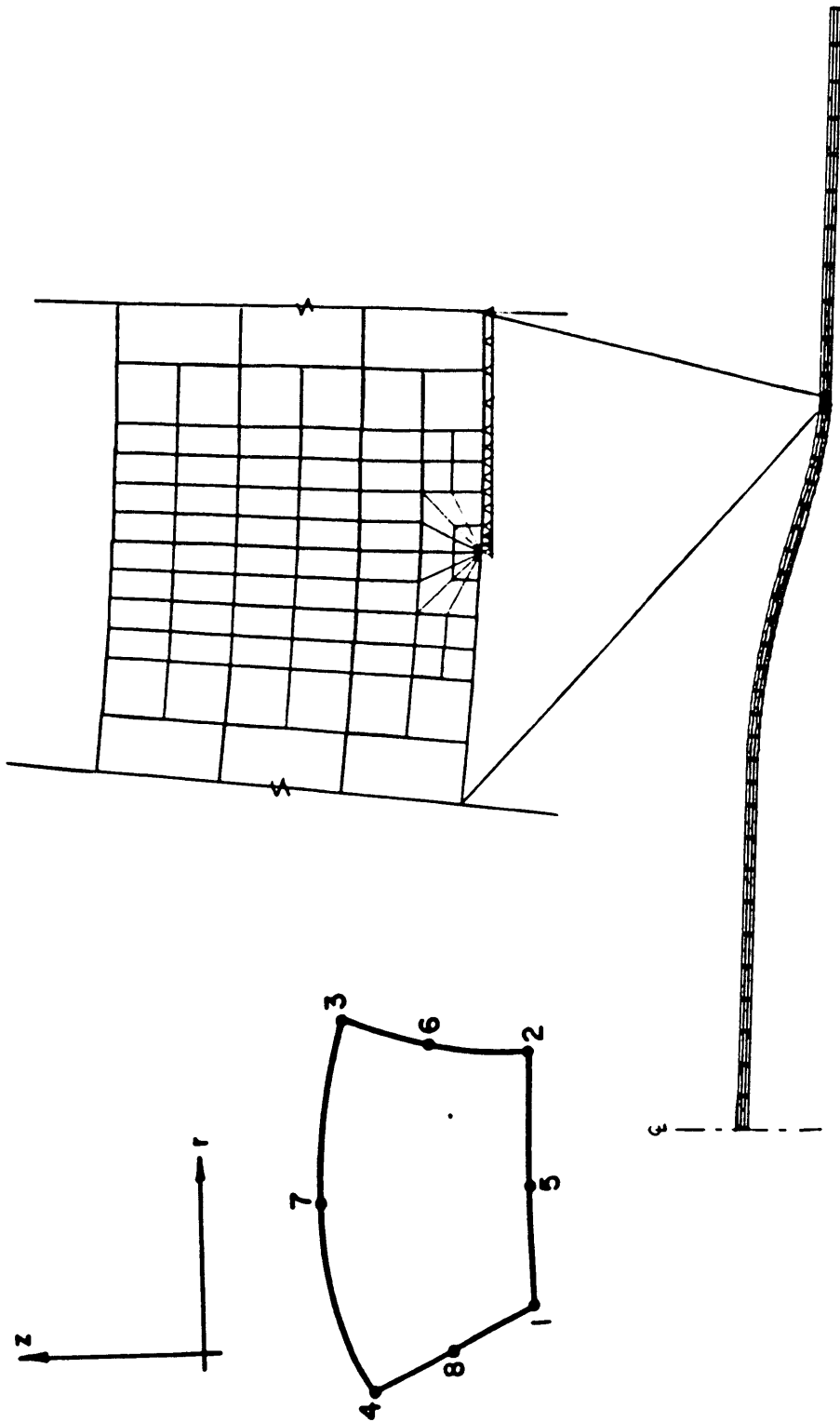


Figure 3.1 Typical element and deformed mesh of the finite element model for an aluminum specimen.

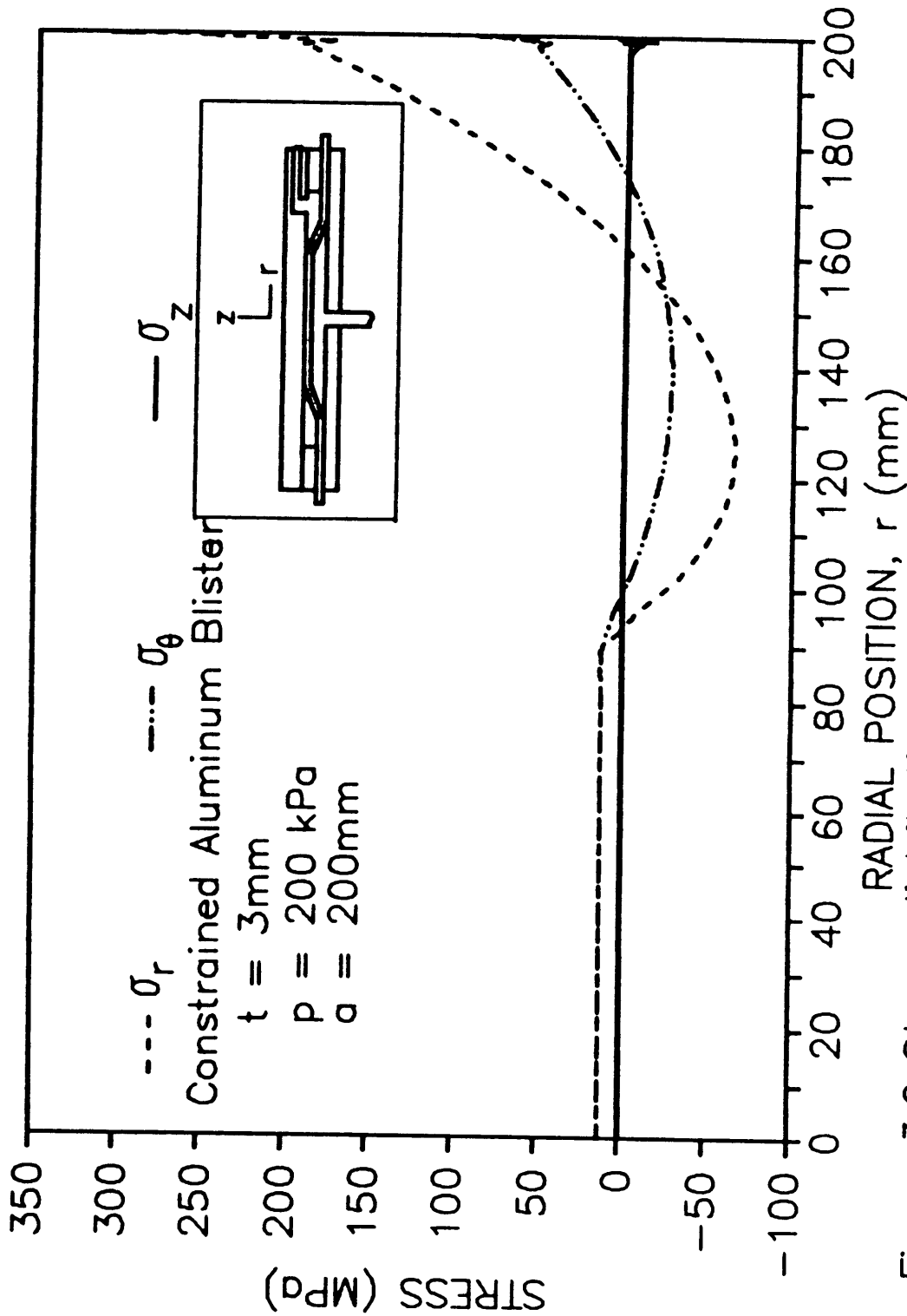


Figure 3.2 Stress distributions along the lower surface of an aluminum specimen using the geometrically nonlinear analysis.

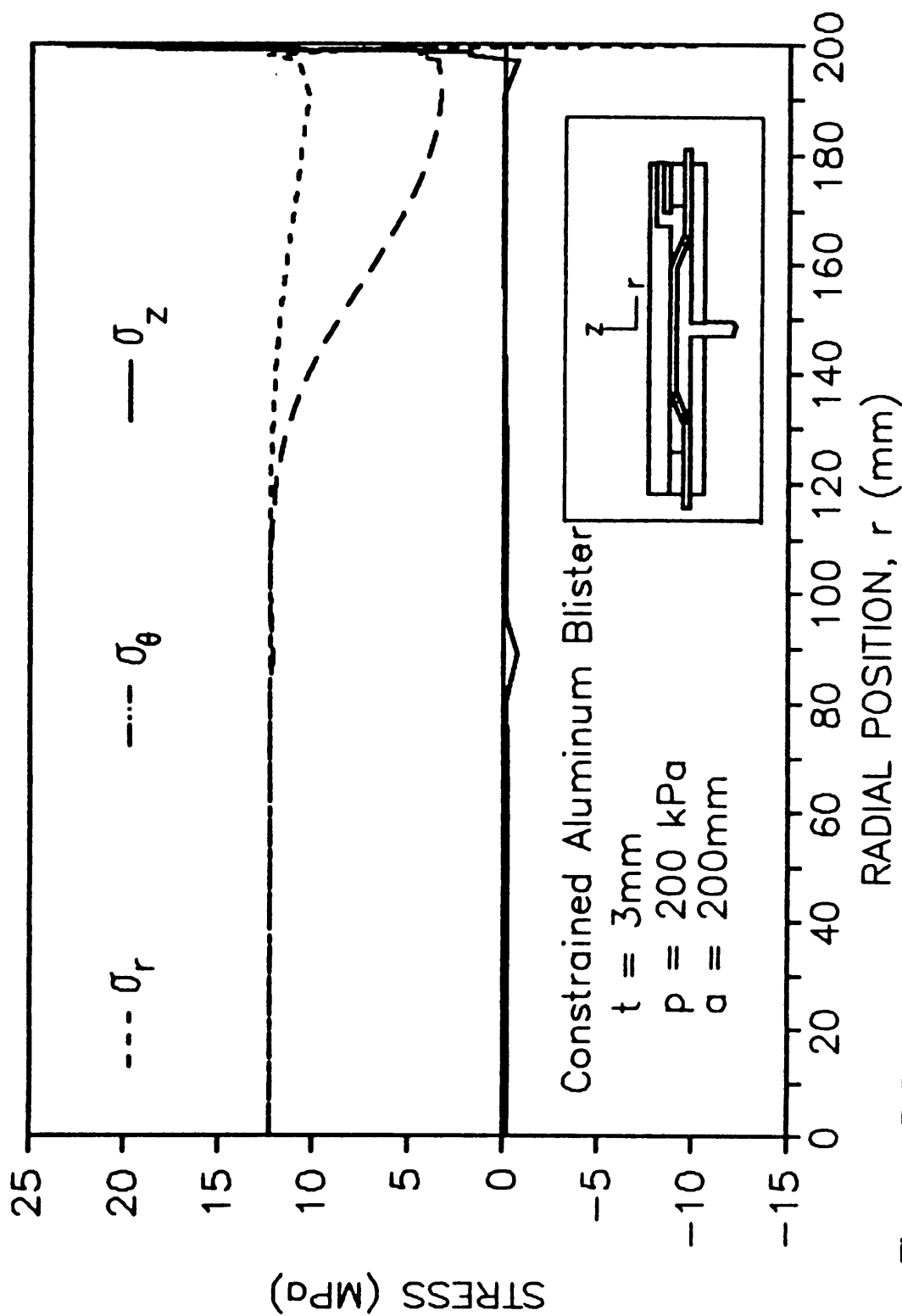


Figure 3.3 Stress distributions of an aluminum specimen at the mid-plane for geometrically nonlinear analysis.

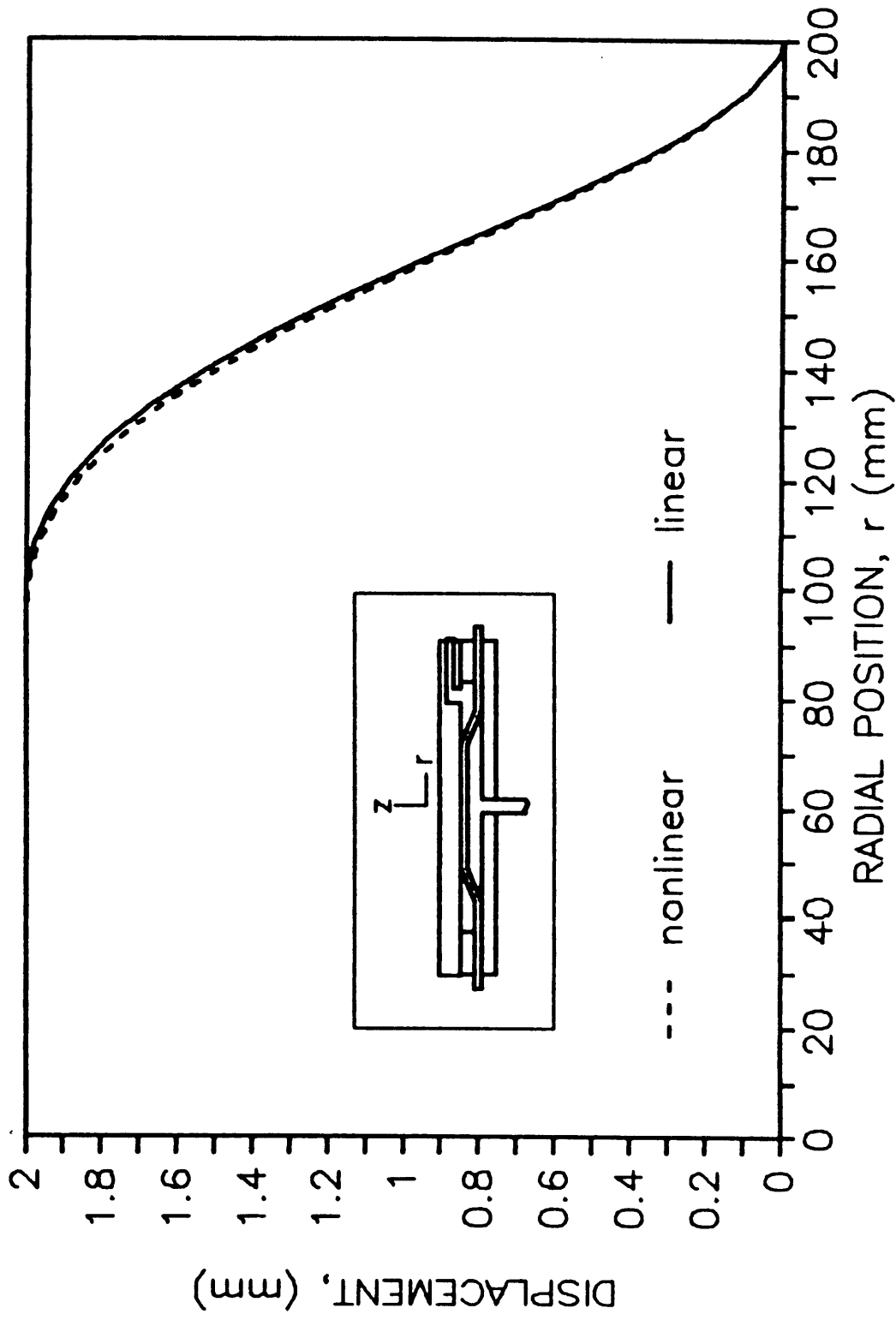


Figure 3.4 Profiles of an aluminum specimen of  $t=3\text{mm}$ ,  $h=2\text{mm}$  and  $p=200\text{kPa}$  for geometrically nonlinear and linear analyses.

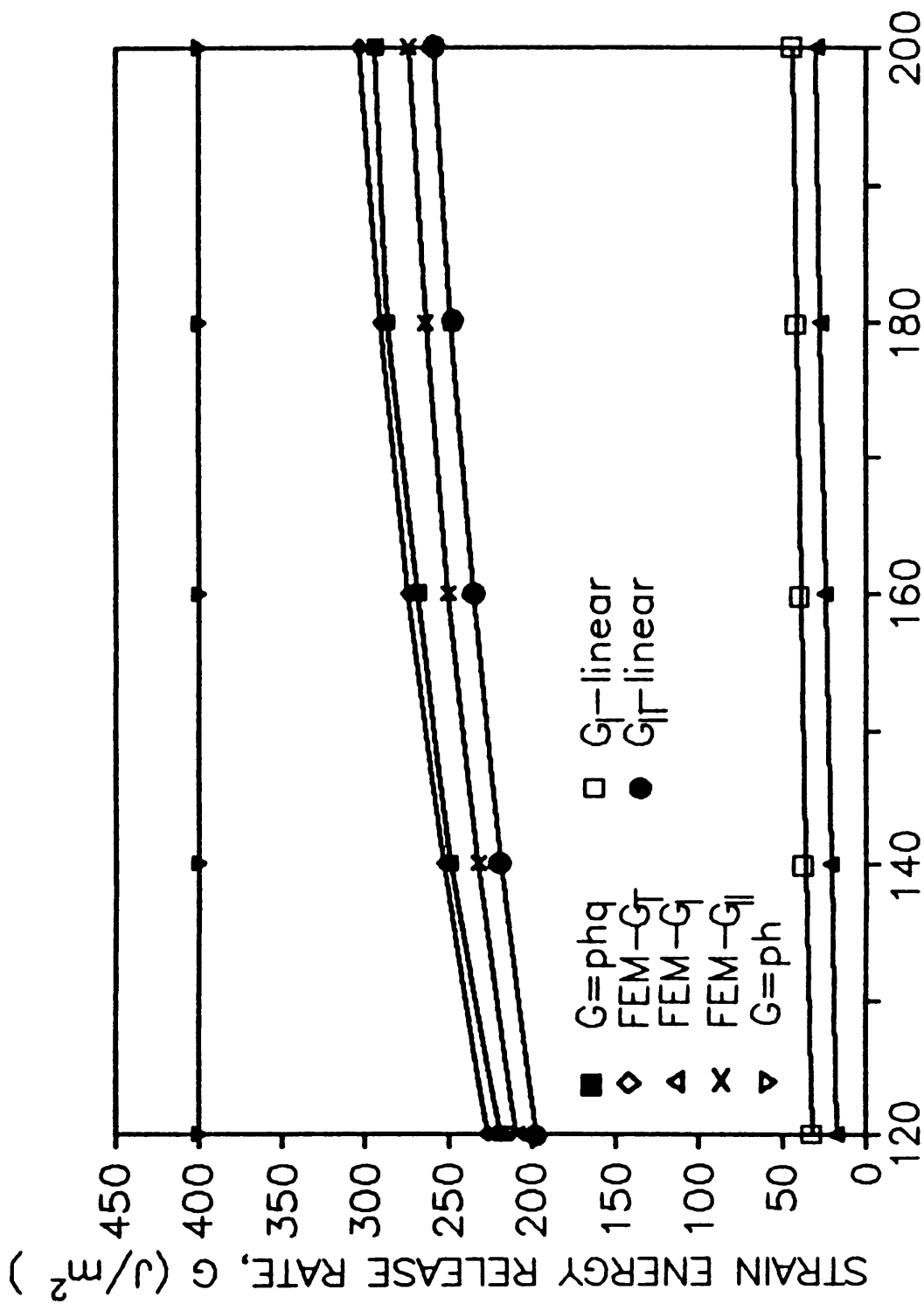


Figure 3.5  $G$  vs  $a$  for an aluminum specimen of  $t=3\text{mm}$ ,  $h=2\text{mm}$  and  $p=200\text{kPa}$ .

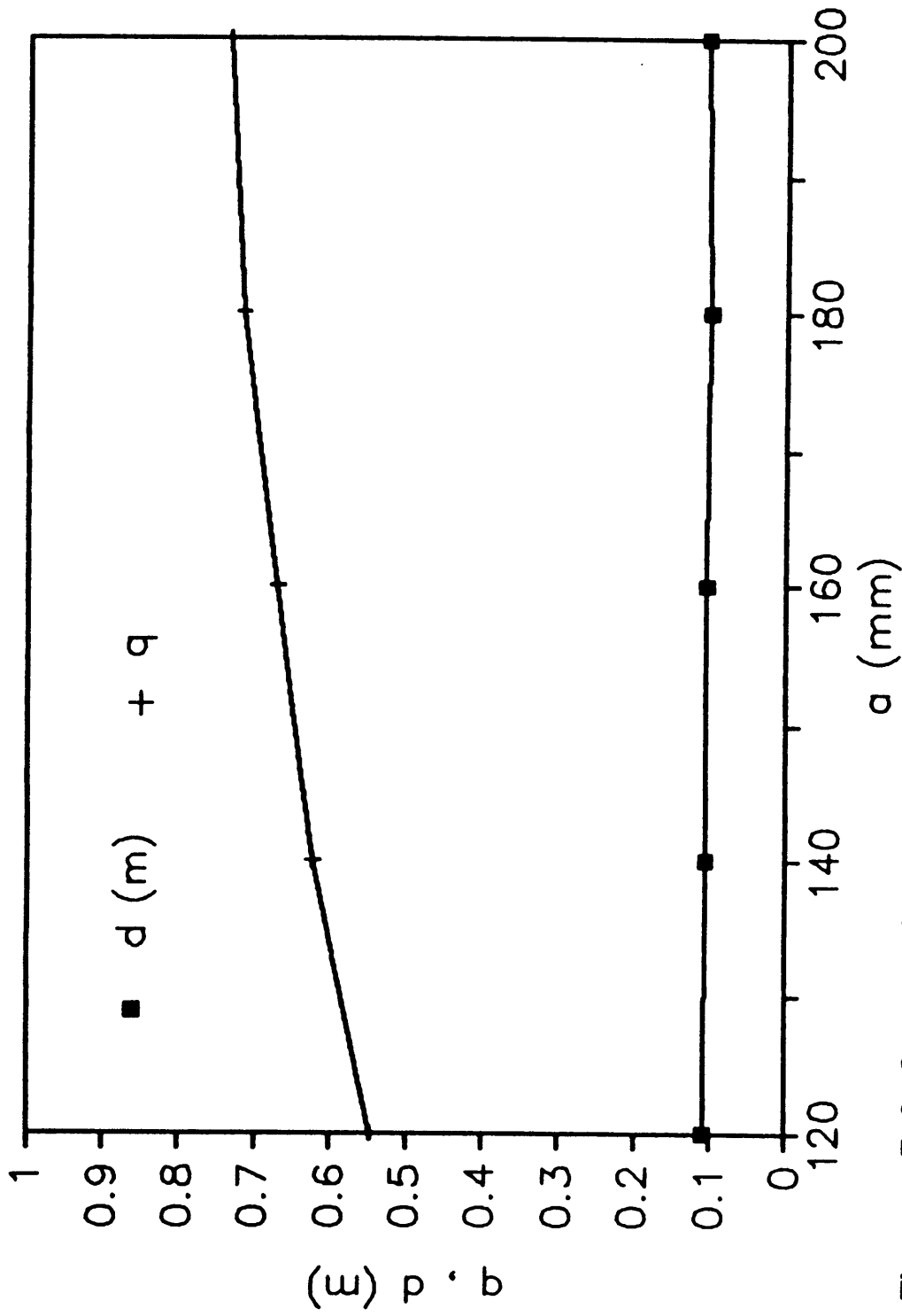


Figure 3.6 Correction factor and the length of suspended region versus debond radius for an aluminum specimen of  $t=3\text{mm}$ ,  $h=2\text{mm}$  and  $p=200\text{kPa}$ .

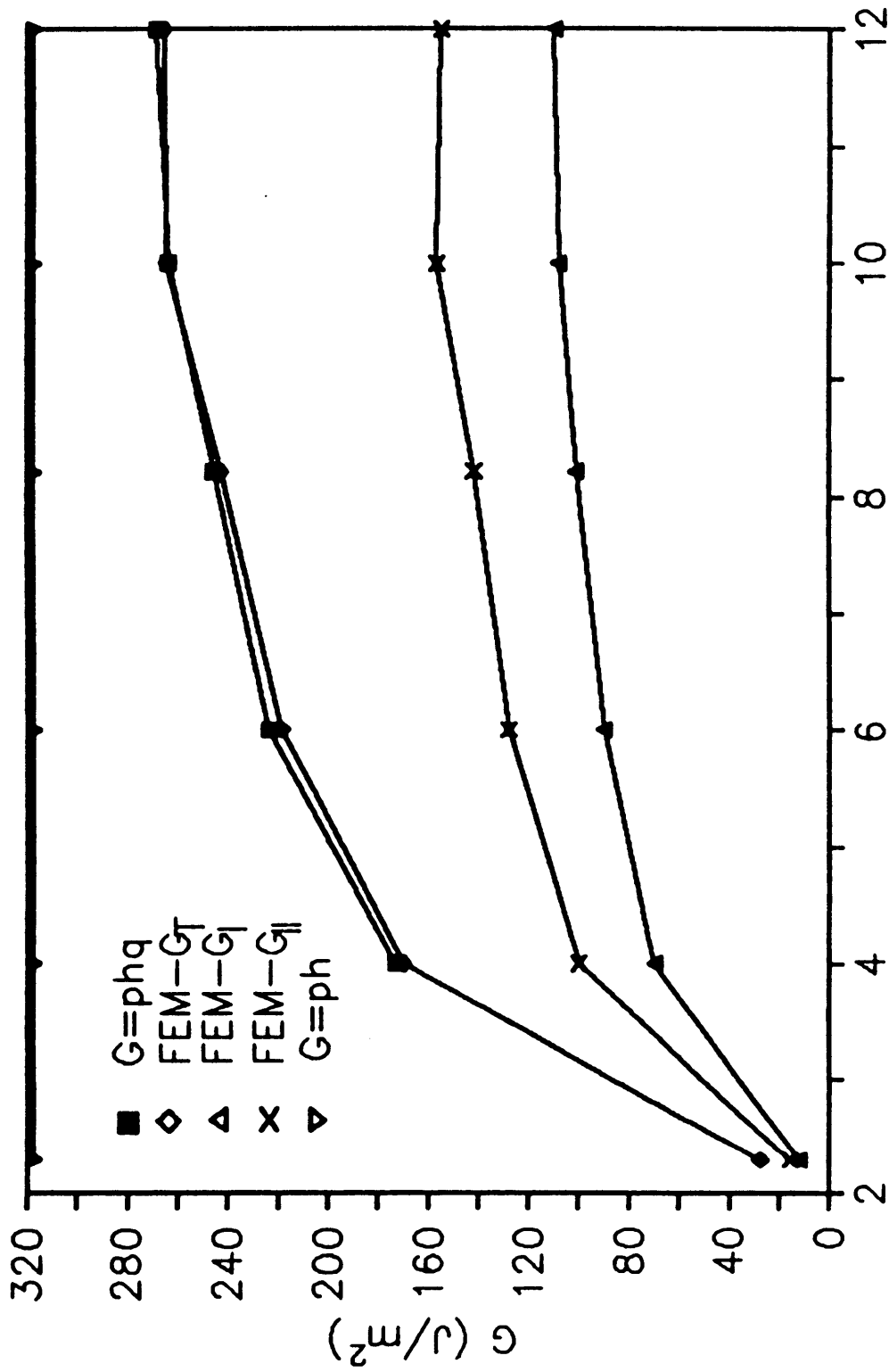


Figure 3.7 G vs a for an adhesive tape of  $t=0.18\text{mm}$ ,  $h=3.175\text{mm}$  and  $p=100\text{KPa}$ .

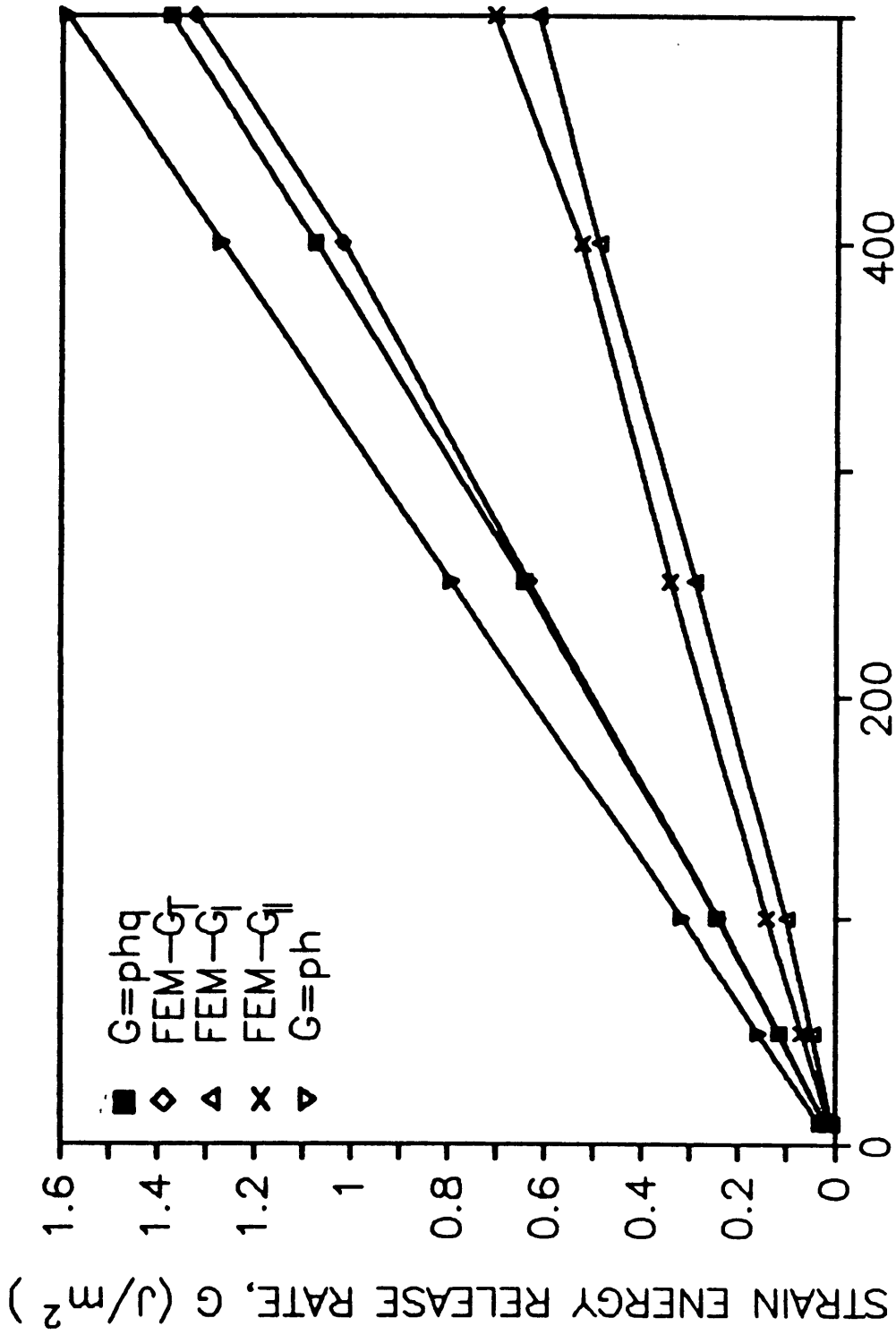


Figure 3.8  $G$  vs  $p$  for an adhesive tape of  $a=8.22\text{mm}$ ,  $t=0.18\text{mm}$  and  $h=3.175\text{mm}$ .

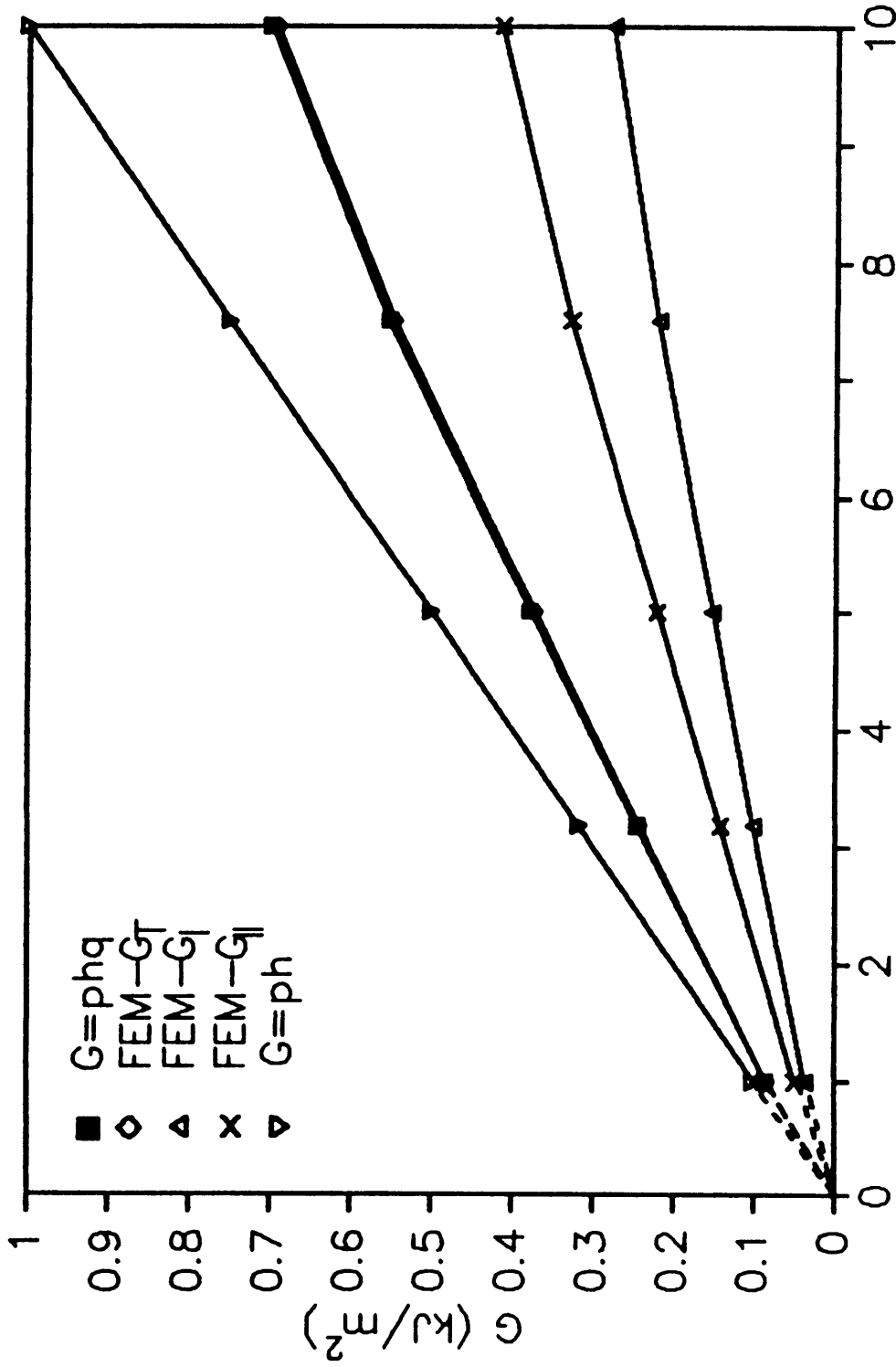


Figure 3.9 G vs h for an adhesive tape of  $a=8.22\text{mm}$ ,  $t=0.18\text{mm}$  and  $p=100\text{KPa}$ .

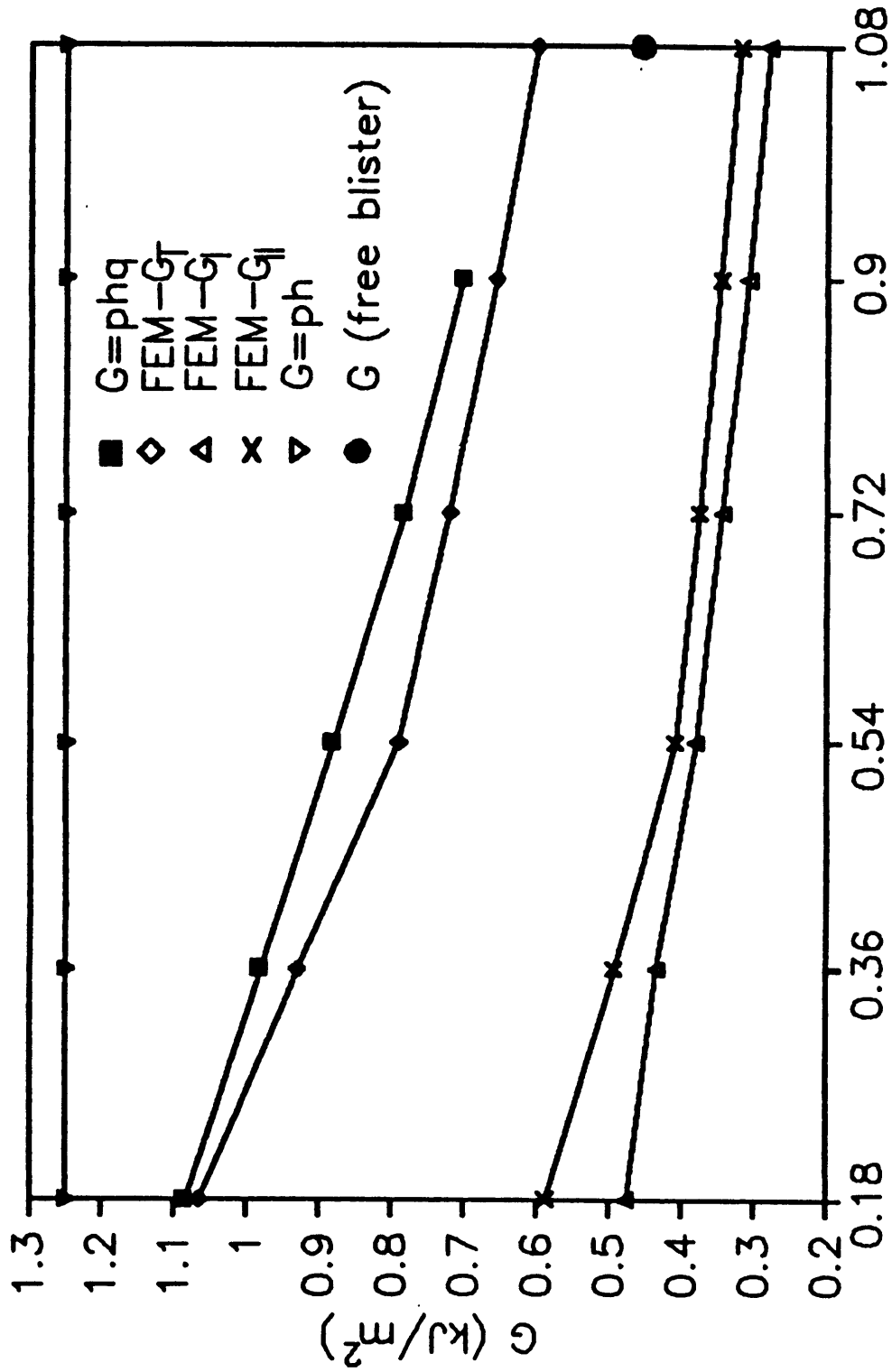


Figure 3.10  $G$  vs  $t$  for an adhesive tape of  $a=8.22\text{mm}$ ,  $h=2.5\text{mm}$  and  $p=500\text{KPa}$ .

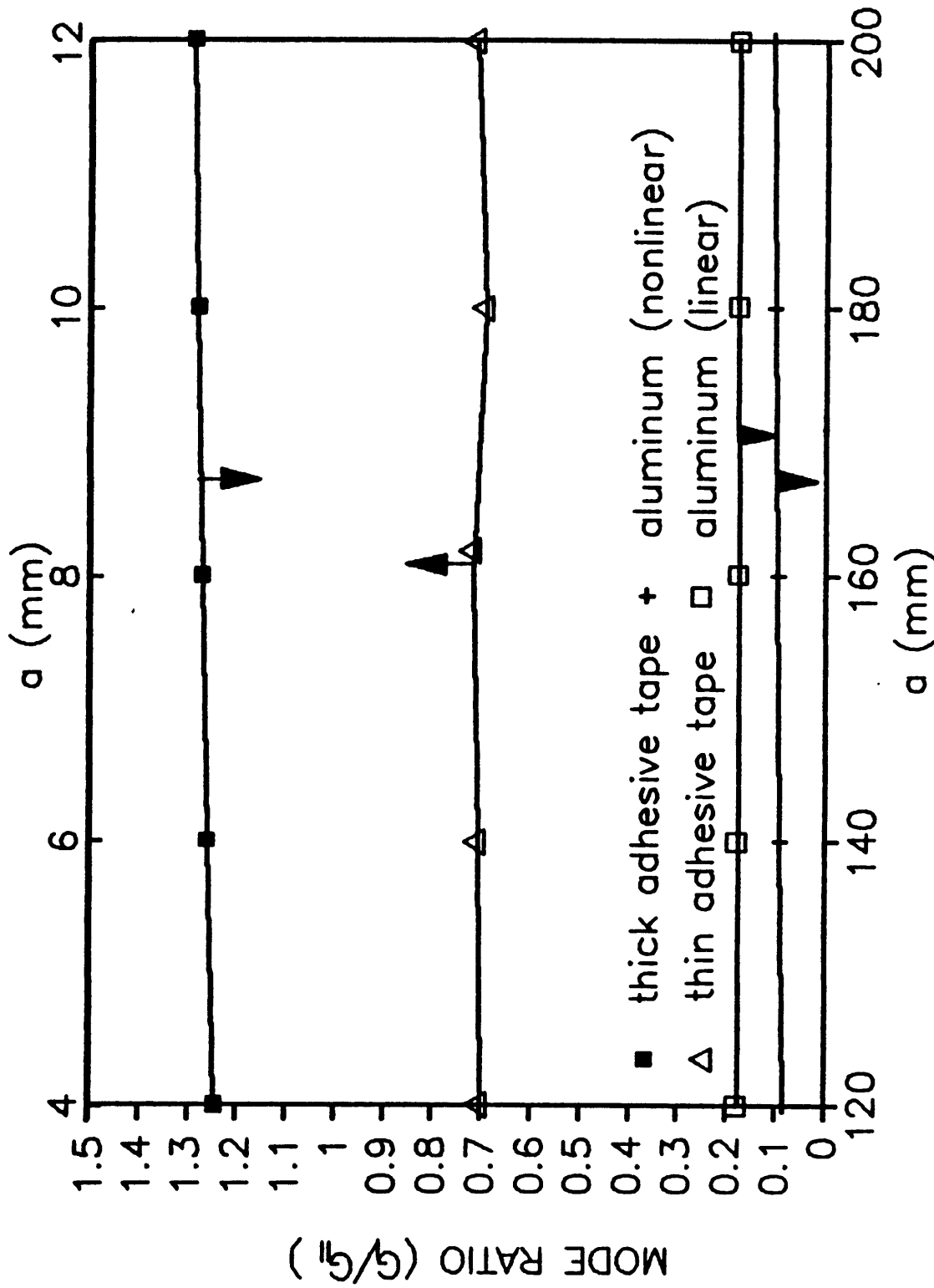


Figure 3.11 Ratios of mode I with respect to mode II for three specimens.

## Chapter 4

### THE APPLICATION OF ELEMENTARY PLATE THEORY TO PREDICT STRAIN ENERGY RELEASE RATE

In Chapter 2, a series of tests on adhesive tapes showed that a state of nearly constant  $G$  was obtained. Numerical analyses in Chapter 3 confirmed the applicability of the approximate solution, Eq. (8), for several typical cases. The numerical analyses also suggested that the determination of the length of the suspended region,  $d$ , and debond radius,  $a$ , are always required in order to accurately estimate the correction factor,  $q$ , and therefore,  $G$ . For thin films or soft specimens,  $a$  and  $d$  can be easily measured by taking pictures through a transparent upper constraint. However, in tests with a stiff specimen such as aluminum, high pressure is required and a rigid opaque constraint such as thick aluminum or steel is needed. In these cases, values of  $a$  and  $d$  cannot be readily obtained. Thus, an alternate technique that can predict strain energy release rate without experimentally measuring  $a$  and  $d$  is developed, and can be used in lieu of the numerical analysis for obtaining the total strain energy release rate.

#### An Elementary Plate Solution for CBT

In the constrained blister test with an elastic specimen, one may neglect the energy dissipation due to far-field viscoelastic effects.

In the test, one may also view the specimen as a thin, flat, circular plate subjected to small deformations, which is the case for a relatively stiff specimen constrained by a small constraint height. Thus the displacement in the radial direction is negligible and one may neglect the slipping and the dissipated frictional energy between the specimen and the upper constraint. Furthermore, if the plastic zone is small compared to the crack length and is localized at the crack tip, which is shown in chapter 3 for an aluminum specimen, one can neglect the dissipated plastic energy. Under the above conditions,  $\delta Z$  term in Eq. (3) can be neglected. Assuming that debonding occurs for all the geometries and loading conditions considered in the following discussions, the critical strain energy release rate will be expressed as energy released due to the variation of the debond area and is given by:

$$G = p \frac{\partial V}{\partial A} - \frac{\partial U}{\partial A} \quad (11)$$

where

$V$  is the volume of the blister, and

$p$  is the pressure which is assumed to be constant in the present discussion.

Although assumed negligible in chapter 2, the variation in strain energy is retained in the present analysis.

If the thickness of the specimen is small in comparison with its radius ( $t \leq \frac{1}{5} a$ ) and the deflection is small compared with its thickness ( $w \leq t$ ), elementary plate theory can be used and the deflection is given as [19,20]:

$$w(r) = C_1 + C_2 \ln r + C_3 r^2 + C_4 r^2 \ln r + \frac{p r^4}{64 D} \quad (12)$$

where

$w(r)$  is the deflection of the plate at any radial position,  $r$ ,

$C_1$ ,  $C_2$ ,  $C_3$  and  $C_4$  are undetermined constants,

$p$  is the uniformly distributed pressure and

$D$  is the bending rigidity which is given as

$$D = \frac{E t^3}{12 (1 - \nu^2)},$$

where

$t$  is the thickness of the specimen,

$E$  is the Young's modulus, and

$\nu$  is the Poisson's ratio.

In the case of a constrained blister, we assume that the edge of the blister is clamped as was done for Eq. (1). In order to determine the four unknown constants and the unknown radius of the inner edge of suspended region,  $b$ , two boundary conditions are applied at the debond

radius, a [19]:

$$(w)_{r=a} = 0 , \quad (13-a)$$

$$\left(\frac{dw}{dr}\right)_{r=a} = 0 , \quad (13-b)$$

and three at the inner edge of suspended region of radius b:

$$(w)_{r=b} = h , \quad (13-c)$$

$$\left(\frac{dw}{dr}\right)_{r=b} = 0 , \quad (13-d)$$

$$(M)_{r=b} = 0 . \quad (13-e)$$

where the last boundary condition, Eq.(13-e) is based on the assumption that just inside the circle of radius b, the slope is zero, therefore, the bending moment must also be zero along this circle, since the inner portion of the plate remains flat.

Thus, a system of five nonlinear equations is obtained to determine the unknown constants and b:

$$C_1 + C_2 \ln a + C_3 a^2 + C_4 a^2 \ln a = - \frac{p a^4}{64 D} \quad (14-a)$$

$$C_1 + C_2 \ln b + C_3 b^2 + C_4 b^2 \ln b = - \frac{p b^4}{64 D} + h \quad (14-b)$$

$$C_1 \frac{1}{a} + C_2 (2a) + C_4 a (2 \ln a + 1) = - \frac{p a^3}{16 D} \quad (14-c)$$

$$C_1 \frac{1}{b} + C_2 (2b) + C_4 b (2 \ln b + 1) = - \frac{p b^3}{16 D} \quad (14-d)$$

$$\begin{aligned} C_2 \frac{\nu-1}{b^2} + 2 C_3 (\nu+1) + C_4 (3 + 2 \ln b + 2 \nu \ln b + \nu) \\ = - \frac{p b^2}{16 D} (3 + \nu) \end{aligned} \quad (14-e)$$

From Ref. 19, the strain energy due to bending can be expressed as:

$$U = \frac{D}{2} \int_b^a \left\{ \left[ \frac{\partial^2 w}{\partial r^2} + \frac{1}{r} \frac{\partial w}{\partial r} \right]^2 - 2(1-\nu) \left[ \frac{\partial^2 w}{\partial r^2} \right] \left[ \frac{1}{r} \frac{\partial w}{\partial r} \right] \right\} dr \quad (15)$$

and the volume of the blister is

$$V = \pi(a-d)^2 h + \int_{a-d}^a 2\pi r w(r) dr \quad (16)$$

Theoretically, by substituting Eq. (12) into Eq. (15) and Eq. (16), differentiating  $U$  and  $V$  with respect to  $A$  and then substituting into Eq. (11), we can obtain the strain energy release rate,  $G$ . However, Eq. (14) is a system of nonlinear equations; obtaining the solutions

in explicit form for the unknown constants and  $b$  is impractical. Consequently, calculating the strain energy release rate numerically is a more practical approach. Fortunately, the numerical library to solve a system of nonlinear equations and do numerical integration is easy to obtain for either a personal or main frame computer.

In the current study, Eq. (14) is solved by using the IMSL [21] subroutine ZSPOW; the bending strain energy,  $U$ , and the volume of blister,  $V$ , are integrated using subroutine DCADRE. By imposing a small variation  $\delta a$  on debond radius, the quantities;  $\delta V$ ,  $\delta A$  and  $\delta U$  are readily obtained. Substituting these quantities into Eq. (11), the strain energy release rate is obtained numerically.

In the following section, predictions of strain energy release rate based on the above algorithm will be compared with finite element predictions for aluminum cases. A simple experimental procedure will also be proposed to predict the strain energy release rate by using this algorithm. The analysis of the constrained blister test based on this algorithm will also be compared with the regular blister test to clarify their differences.

### Results and Discussions

Figures 4.1 to 4.4 are the predictions of the plate theory compared with those of finite element analysis with the geometrically nonlinear option for an aluminum 6061-T6 specimen which has a thickness of 3mm,

a constraint height of 2mm, and is subjected to a pressure of 200kPa. The finite element program called ABAQUS, which is capable of handling contact problems, was used (version 4-5-154). In these figures, the legends denoted 'FEM' and 'PLATE', represent the predictions of finite element analysis and elementary plate solution, respectively.

Figure 4.1 illustrates a typical deformed profile at the midplane of the specimen for an aluminum specimen of  $a=200\text{mm}$ . Excellent agreement is seen between the predictions of the geometrically nonlinear finite element analysis and elementary plate theory. It is noted that according to Ref. 19, if there were no upper constraint, the deflection of a plate of the same geometry subjected to this loading condition would be so large that the problem would need to be treated as a large deformation plate problem and the deviation of deflection at the center from elementary plate theory with respect to that from an approximate solution of large deflection plate theory would be around 400%. The excellent agreement in Fig.4.1 shows that the upper constraint has prevented membrane effects from significantly stiffening the plate. The elementary plate theory solution which ignores membrane effects and shear deformation agrees very well with the finite element solution which accounted for geometric nonlinearities and shear deformation. This also suggests that the effect of shear deformation is not significant. It should also be noted that for this geometry, the nonlinear and linear finite element analyses have similar deformed profiles but have different stress

distributions.

Figure 4.2 illustrates the stress distribution in the radial direction at both the top and bottom surface of the specimen. It should be noted that the stress distributions from both elementary plate theory and finite element analysis do not exceed the yielding point except for the region very near the crack front which has a singular point (about 0.05% of the thickness). It is seen that the stresses from the elementary plate theory are higher than those of the finite element analysis in the suspended region. In the contact region, however, the stresses from the elementary plate theory are smaller. The reason for the former phenomenon is due to the assumption that the outer edge is fixed at  $r=a$  in the elementary plate approach, which provides a stiffer constraint than exists in the real specimen analyzed in the finite element model, and thus causes higher bending moment and stresses. The reason for the latter phenomenon is due to the assumption of the small deformation for the elementary plate theory which results in zero stresses at the mid-plane of the specimen, where the finite element analysis shows non-zero membrane stresses. Although the predicted stresses deviate substantially, it will be shown that the stored energy is small in comparison to input work, thereby minimizing errors in predicted strain energy release rates.

Although the finite element results did not show the oscillation of

the displacement at  $r=b$ , a small oscillation of the stress distribution in the  $r$  direction,  $\sigma(r)$ , did reveal that very localized oscillation occurs Fig.3.3 . However, the excellent agreement of the displacement profile suggests that  $(M)_{r=b}=0$  is a good assumption as well as the fixed end assumption at  $r=a$ .

Figure 4.3 illustrates volume of the blister versus debond radius. Excellent agreement is seen. For  $a < 102\text{mm}$ , the elementary plate solution indicates that the specimen does not touch the upper constraint and suggests that initial debond radius in the constrained blister test should be larger than 102mm.

Figure 4.4 illustrates the strain energy release rates versus  $a$ , using the results from the finite element analysis, approximate solution, Eq. (8), and elementary plate theory. The variation of input work on the system and the variation of strain energy from Eq. (11), based on elementary plate theory, are also shown in the figure to indicate the relative magnitude of the bending strain energy. The legends, 'G-PLATE', 'G=phq', and 'FEM', represent the energy release rates obtained from the elementary plate theory, approximate solution (Eq. 8) and the finite element analysis, respectively. Another two legends, 'dW/dA-PLATE' and 'dU/dA-PLATE', represent the variation of work on the system and the variation of the strain energy of the specimen from the elementary plate theory, respectively. The calculations were performed at a strain energy release rate which is

typical aluminum bonding [7]. It is noted that the strain energy release rates from the elementary plate theory are smaller than the FEM predictions. The difference appears to arise because the analytical solution predicts higher stresses, as shown in Fig. 4.2, and thus, variation in strain energy,  $\partial U/\partial A$ , than the FEM results. On the other hand, the FEM results include  $\partial U/\partial A$  term for the membrane effects which are not include in plate theory. However, from Chapter 2, it is shown that the variation of the strain energy is only a small fraction of the variation of the input work. Thus the error from the stress prediction does not induce a large error when the total strain energy release rate is calculated, because the first term on the right hand side of Eq. (11),  $p \frac{\partial V}{\partial A}$  ( $= \frac{\partial W}{\partial A}$ ), is the dominant term and is shown to be very accurate from the volume prediction from the elementary plate theory in Fig. 4.3. It is also seen in this figure that the approximate solution,  $G=phq$ , is a good approach if one can obtain the debond radius and the length of the suspended region, which are obtained from the finite element results in the current comparisons. All three approaches show that the rate of increase of  $G$  decreases as debonding proceeds, and a nearly constant  $G$  is seen at large values of debond radius.

Figures 4.3 and 4.4 also offer us an efficient way to predict the debond radius and the strain energy release rate in a constrained blister test. The prediction procedures are illustrated in Fig. 4.5 and stated as follows: First of all, use the algorithm developed in

the previous section to run several cases for different parameters such as  $p$ ,  $h$ ,  $t$ , and  $a$  for the selected specimen geometries to determine the conditions for the existence of contact between the specimen and upper constraint. Secondly, run several cases with different  $a$ 's to obtain the figures of "volume vs  $a$ " and " $G$  vs  $a$ ". Thirdly, perform the experiment with the initial debond size predicted from step 1 and measure the blister volume. Finally, from the figure of "volume vs  $a$ ", one can determine the debond size and refer to the figure of " $G$  vs  $a$ " to obtain the  $G$  for the specific  $a$ 's. Using these procedures, the strain energy release rate is easily determined and automated evaluation is possible.

Although the theoretical background of the current approach is confined to small deformation plate theory, it is reasonable that if the loading condition and specimen geometry result in a small length for the suspended region, the error for volume predictions between the elementary plate approach and nonlinear finite element analysis would be small even for the constraint height larger than the blister thickness. Since the variation of input work is the dominant term determining the strain energy release rate, the error induced from the increasing membrane strain energy may be still relatively small when determining the total strain energy release rate. Because a nondimensionalized and explicit form solution of the constrained blister test could not be obtained in the current study, the complete criterion of the applicability of the elementary plate theory for the

constrained blister test could not be established. However, by increasing the constraint height,  $h$ , beyond the limitation of the small deformation plate theory, one can obtain a greater understanding of the limitations of the proposed approach. Figure 4.6 illustrates the strain energy release rate versus constraint height for both geometrically nonlinear finite element analysis and elementary plate approach for the same aluminum specimen analyzed previously. The applied pressure is 1MPa. It is seen that the prediction of  $G$  from plate theory has only 5.3% deviation even for an  $h$  which is four times the thicknesses. It should be noted that at  $h=5t$  for this geometry, the specimen does not touch the upper constraint, thus no further comparison is shown in the figure. It is also seen that the rate of change of  $G$  obtained from FEM predictions decreases as  $h$  increases, while that from plate theory does not. This suggests that the membrane effect increases as  $h$  increases and larger deviation is expected for  $h>4t$ .

Although Fig.4.6 shows that the strain energy release rate is still accurate when  $h$  is four times the thickness, the predictions of the blister volume are not as accurate as those of strain energy release rate. Figure 4.7 shows the volume of the blister versus the constraint height. It is seen that the accuracy of volume prediction decreases as  $h$  increases, which is due to the increase of the membrane effect considered by the FEM analysis. At  $h=3t$ , the deviation of the volume prediction from the plate theory is about 12% from the FEM analysis.

It is noted that the strain energy release rate predictions have higher accuracy than volume predictions. The phenomenon can be explained in that even though the accuracy of the volume predictions decrease for larger  $h$ , the variations of the volume are about the same from the elementary plate and FEM predictions under a small increment of debond radius,  $\delta a$ , and thus results in better prediction for the variation of input work and the strain energy release rate.

Figure 4.8 illustrates the variation of the strain energy release rate based on plate theory as the debond grows for the same aluminum specimen as in Figs. 4.1-4.4. The variations of work input on the system and strain energy as the debond grows are also illustrated. The results from the regular blister test and constrained blister test are noted as '-BT' and '-CBT' in the figure. When  $a$  is smaller than 102mm, the deflection at the center of the plate calculated from elementary plate theory [19]:

$$w = \frac{1}{64} \frac{p}{D} a^4 \quad (17-a)$$

is smaller than the constraint height, and the radius of the contact region,  $b$ , calculated from Eq. (14) is smaller than 0. Both results show that the specimen does not touch the upper constraint. On the other hand, for  $a > 102\text{mm}$ , both results indicate that the specimen contacts the upper constraint. Thus, for  $a < 102\text{mm}$ , the specimen is a regular blister and the strain energy release rate is calculated from

Eq. (11) which has  $\frac{\partial U}{\partial A} = \frac{1}{2} p \frac{\partial V}{\partial A}$  and thus [19]:

$$G = \frac{3}{32} \frac{(1-\nu^2)}{E t^3} p^2 a^4 \quad (17-b)$$

It is clearly seen that for  $a < 102\text{mm}$ ,  $G$  is a function of  $a^4$  and small errors of measuring debond radius would cause large errors in  $G$ . For  $a > 102\text{mm}$ , the specimen becomes a constrained blister and  $G$  is calculated from the approach proposed in the previous section. It is seen that small errors in measuring or estimating debond radius would not induce the large errors in  $G$  as would the regular blister test. It is also seen that the variation of the strain energy term in Eq. (11) is more important in the regular blister approach, while it is less important in the constrained blister approach.

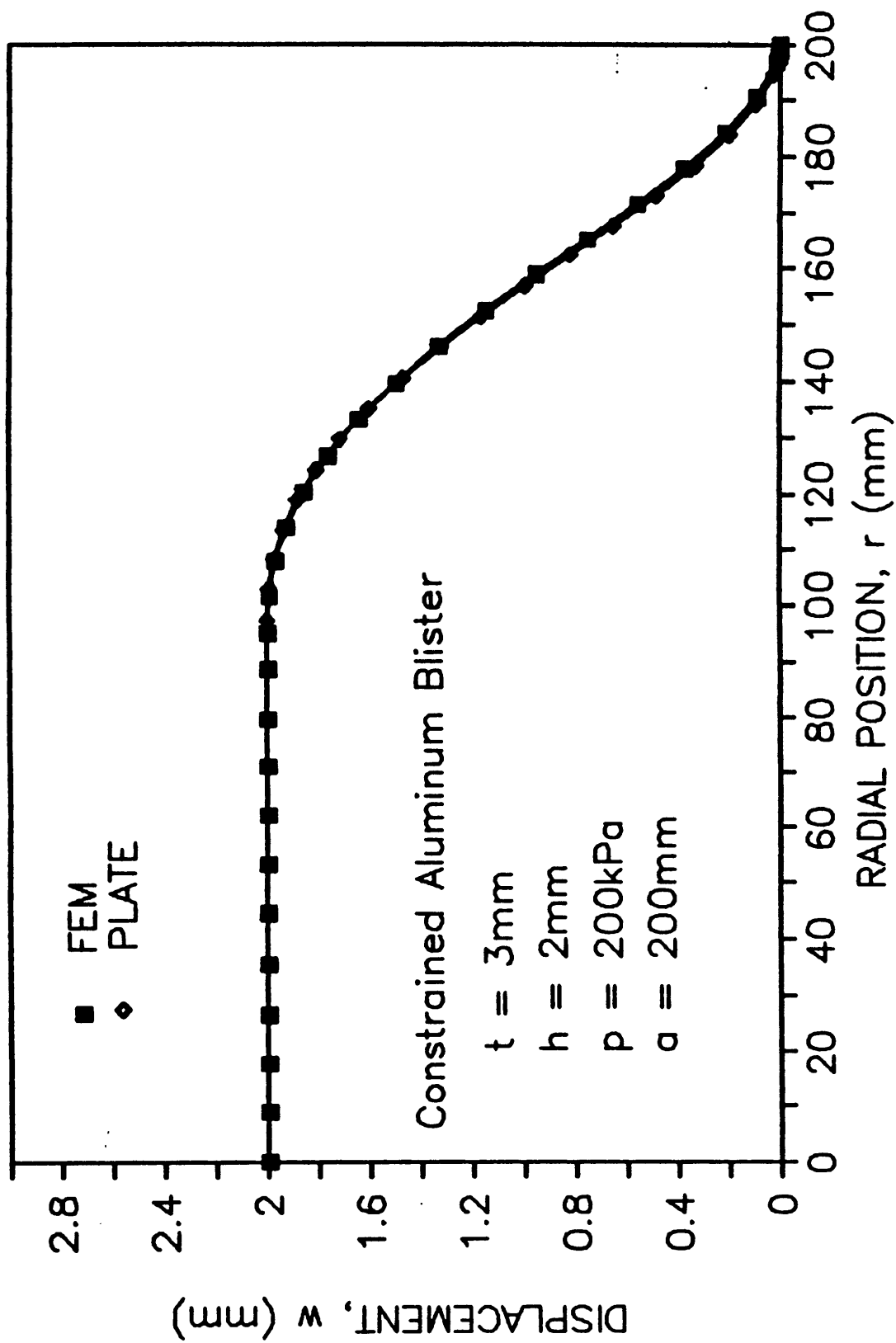


Figure 4.1 Profiles of an aluminum specimen for the analyses of FEM and plate theory.

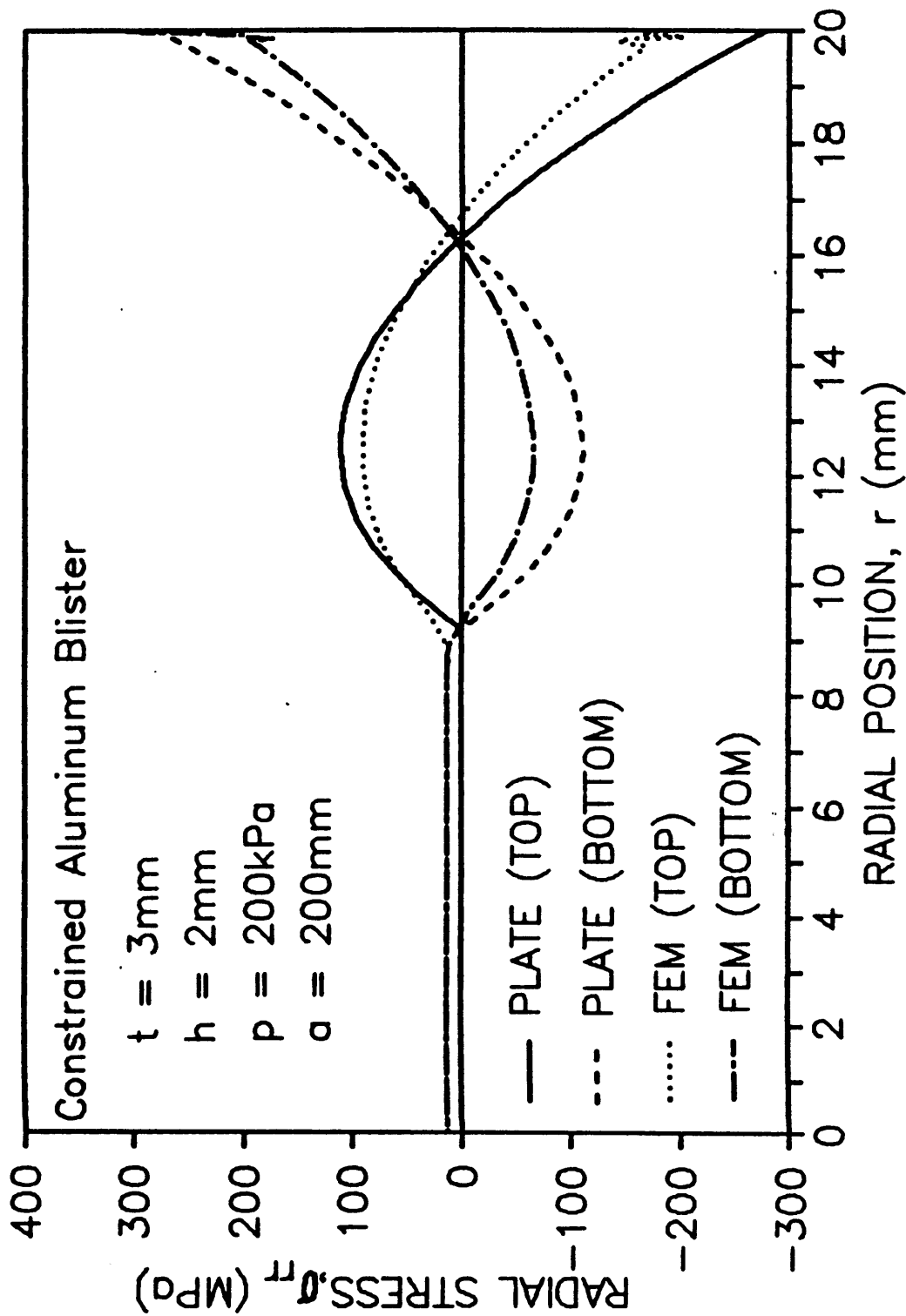


Figure 4.2 Radial stress distribution predicted by FEM and plate theory along the top and bottom surfaces of an aluminum specimen.

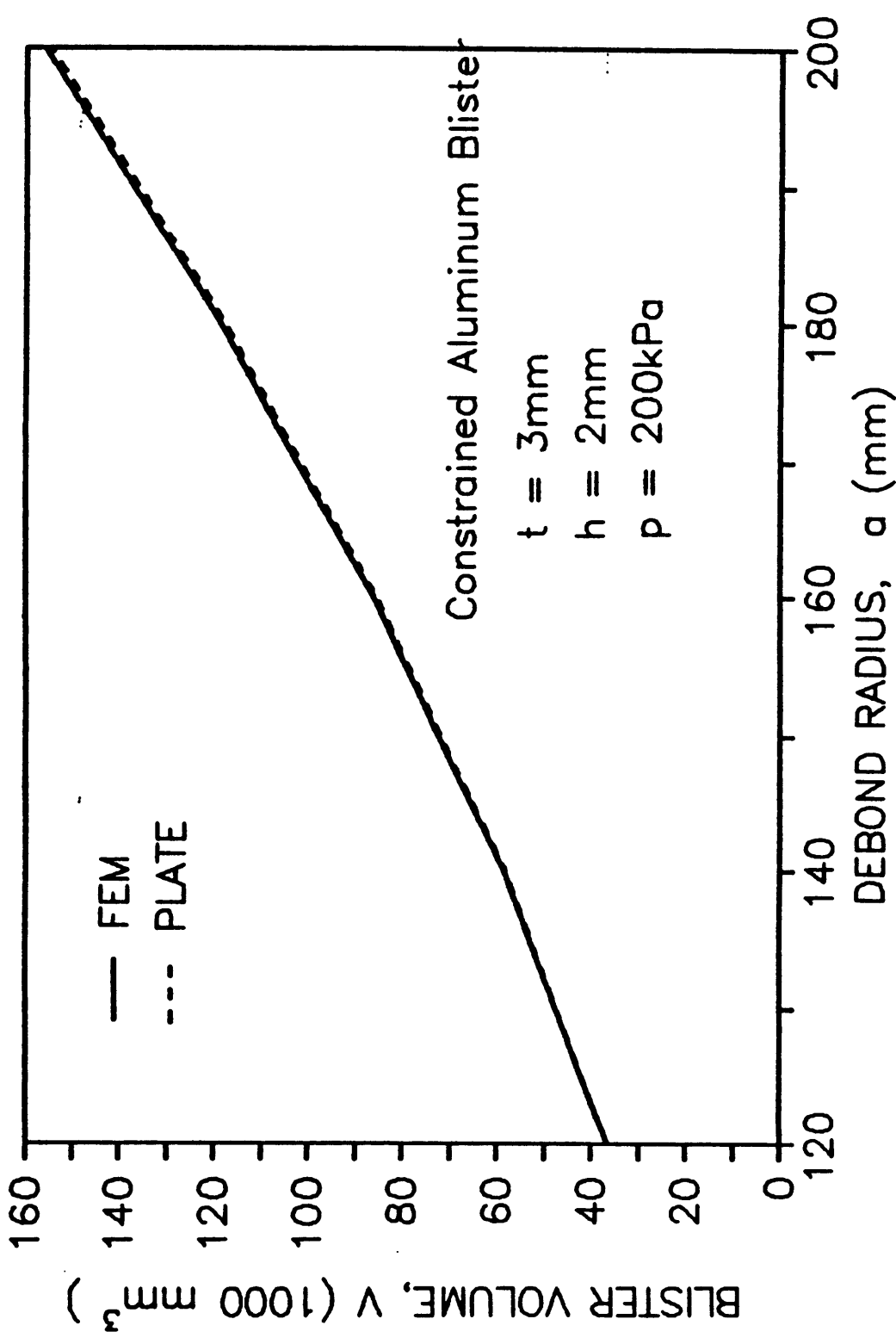


Figure 4.3 Volume of the blister versus debond radius predicted by FEM and plate theory for an aluminum specimen.

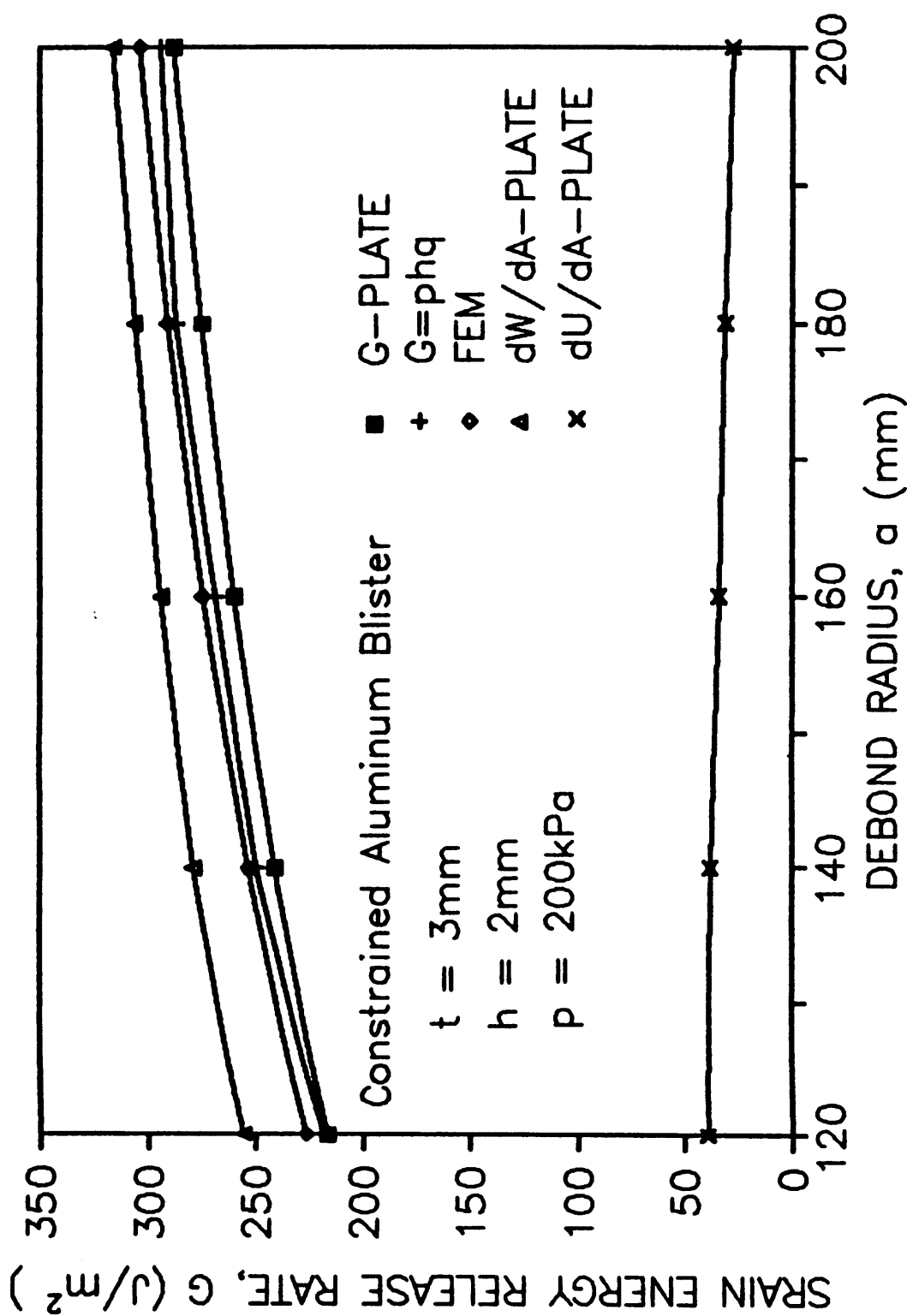


Figure 4.4 Strain energy release rates versus debond radius for an aluminum specimen.

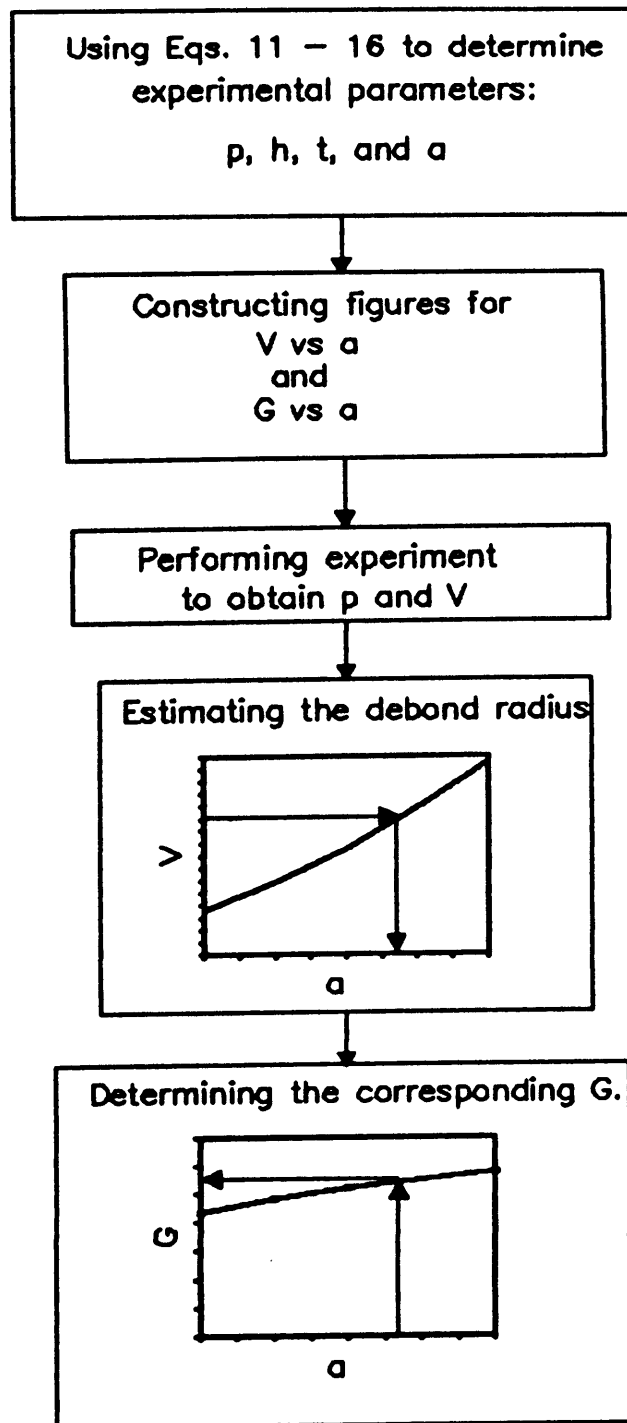


Figure 4.5 The automated algorithm to determine  $G$ .

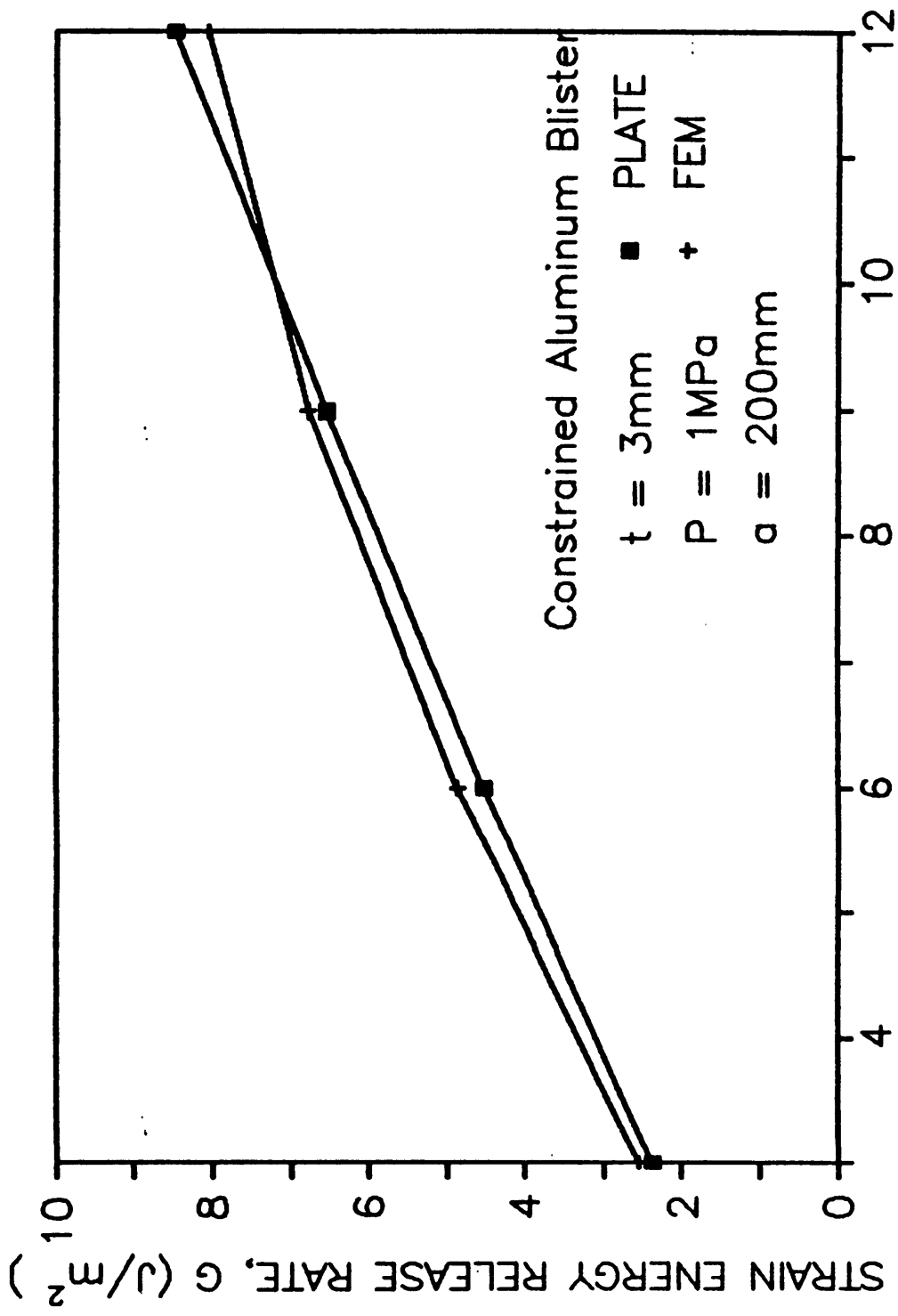


Figure 4.6 Strain energy release rates versus constant height predicted by FEM and plate theory for an aluminum specimen.

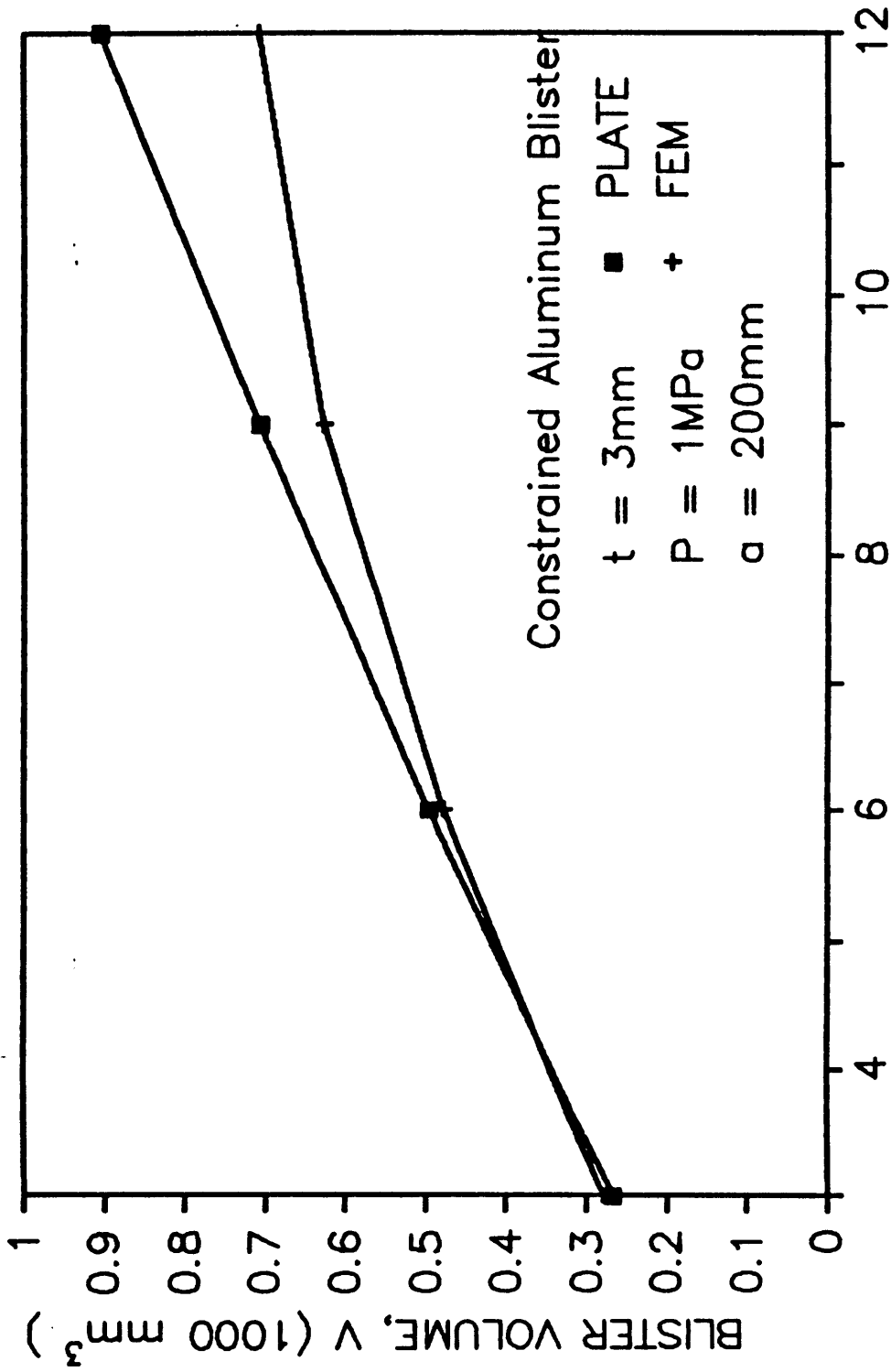


Figure 4.7 Volume of the blister versus constraint height predicted by FEM and plate theory for an aluminum specimen.

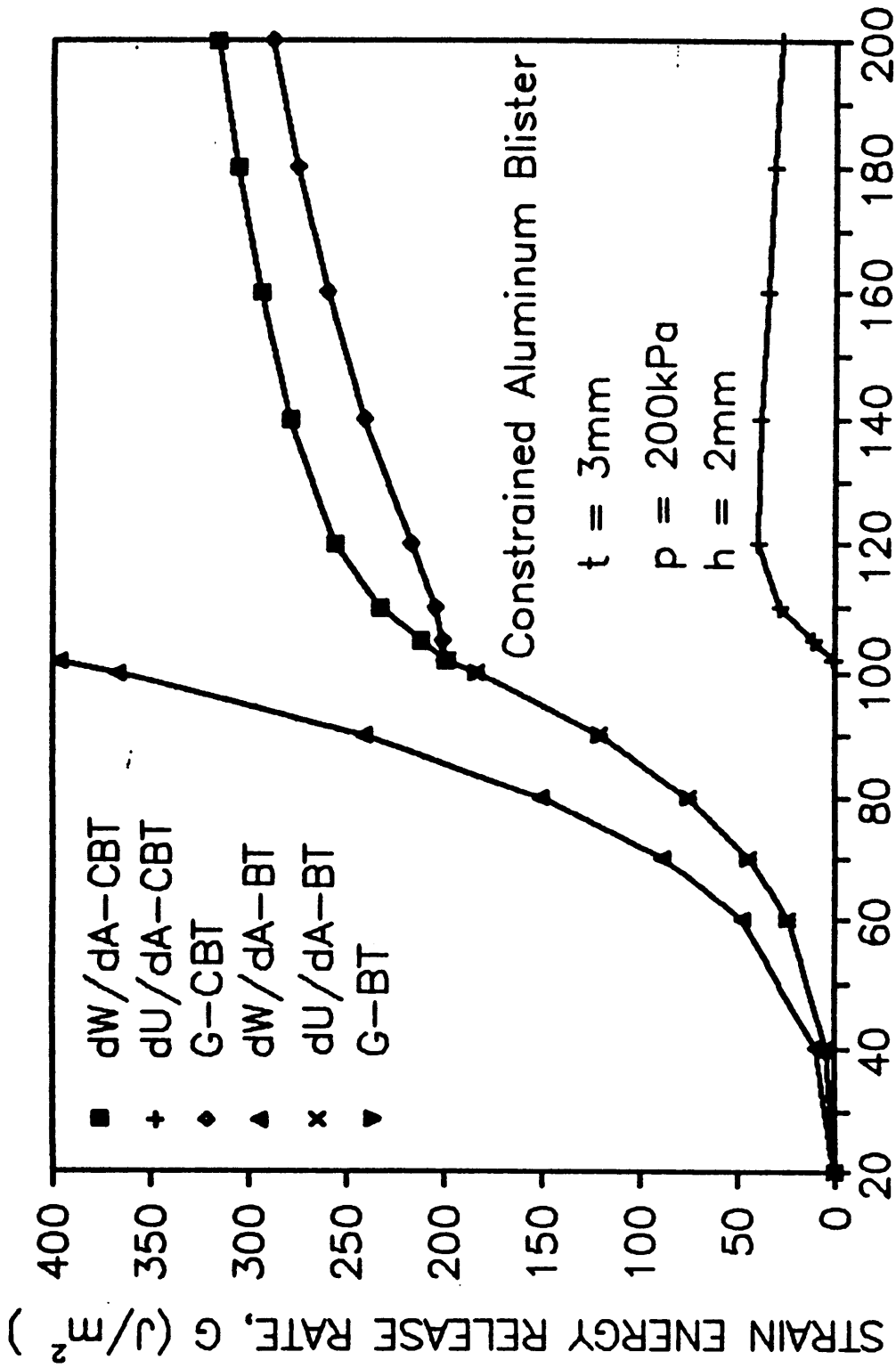


Figure 4.8 Illustration for the variation of  $G$  during the debonding process for a constrained blister test with a regular blister as  $a$  is smaller than 102mm.

## Chapter 5

### SUMMARY, RECOMMENDATIONS, AND CONCLUSIONS

#### Summary of Work

This study developed and analyzed the constrained blister test (CBT), which is a modification of the blister test permitting nearly constant strain energy release rate testing of adhesive bonds. The work consisted of three parts; (1) the development of the testing technique to evaluate strain energy release rate and to record the time-dependent nature of the fracture process, (2) the numerical analysis of the constrained blister test to determine the applicability of an approximate solution for several materials, and (3) the development of an analytical technique to evaluate the strain energy release rate for relatively stiff specimens. The work is summarized in the following sections.

In the first part of the study, a testing procedure and an approximate solution were established, and two adhesive tape systems were investigated using this technique. The results of polyester tape suggest that at a constant pressure, the radius of the blister increases linearly with time, which results in a stable debonding process. The validity and reproducibility of the constrained blister test were also successfully confirmed by comparing with the free membrane blister test and standard peel tests with different take-off

angles. For the vinyl tape tested, however, the rate of debonding of the radius was not constant. Instead, the rates decreased as the blister grew. This behavior was attributed to the significant creep of the vinyl backing material and suggested the necessity of proper inclusion of viscoelasticity into the debond model for this material system.

In the second part of the study, a series of finite element analysis were performed to verify the applicability of the approximate solution for the constrained blister test. Typical materials and geometries were chosen to examine the effects of the parameters such as pressure, constraint height, debond radius, thickness of the specimen and material properties. Although some problems were encountered using the current version of ABAQUS, the results suggested that the CBT technique successfully dealt with the problems of various material properties and specimen dimensions.

An approach based on elementary plate theory to evaluate the strain energy release rate in the constrained blister test was studied in the last part of the work. This approach is especially applicable for relatively stiff blister specimens, such as metallic specimens, which are not suitable for visual observation of the debonding process. The strain energy release rates predicted from this approach are in good agreement with those predicted from the finite element analysis and the proposed approximate solution. Although elementary plate theory is

only applicable when the maximum deflection is smaller than the thickness of the plate, The results of an aluminum specimen suggest that the proposed approach is applicable for the cases with the constraint height larger than the specimen thickness, under the appropriate loading and geometrical conditions. In the experimental scheme of the constrained blister test proposed in this paper, only the volume and the pressure difference between the inside and outside of the blister need to be measured during the debonding process. The measurements are easy to perform and may be automated when combined with the proposed approach.

In summary, a technique with nearly constant strain release rate has been successfully developed in this study. Numerical analysis confirmed the applicability of the approximate solution. In addition, the analytical approach based on elementary plate theory offers a practical and efficient way to estimate strain energy release rate for metal adherends and suggests wider applicability of the constrained blister technique.

### Recommendations

While most of the objectives of this study were accomplished, there are still many improvements which need to be made in the future. The most noticeable ones are: (1) to properly include the viscoelasticity into the debond model for this material system, (2) to successfully use the nonlinear geometrical option of finite element analysis to

analyze the membrane type specimens, (3) to properly define the limitations of the elementary plate approach used in the constrained blister test, (4) to perform more tests with the metal and other specimens to confirm wider applicability of the constrained blister test.

### Conclusions

The constraint adds a new dimension to fracture testing because it provides a means to obtain a constant strain energy release rate test by limiting the amount of stored energy to a very small fraction of the work done under constant load conditions. The preliminary experimental, numerical, and analytical results suggest that the advantages of nearly constant strain energy release rate with nearly constant mode ratio and automatic measurement have made the constrained blister test a potentially useful testing technique for adhesives.

## References

1. S. Mostovoy and E. J. Ripling, Final Report, "Fracturing Characteristics of Adhesive Joints", Contract No. N00019-74-c-0274. Mater. Lab., Glenwood, Illinois, 1975.
2. G. P. Anderson, K. L. DeVries, and M. L. Williams, "Mixed Mode Stress Field Effect in Adhesive Fracture", Int J Fract, 10 (5), 1974, pp.565-583.
3. H. Dannenberg, "Measurement of Adhesion", J Appl Polym Sci, 5, 1961, pp.125-134.
4. M. L. Williams, "The Continuum Interpretation for Fracture and Adhesion", J Appl Polym Sci, 13, 1969, pp. 29-40.
5. D. R. Lefebvre, D. A. Dillard and H. F. Brinson, "The Development of a Modified Double Cantilever Beam Specimen for Measuring the Fracture Energy of Rubber to Metal Bonds", Experimental Mechanics, 28, (1), 1988, pp. 38-44.
6. W. B. Jones, "Cohesive and Adhesive Polymer Fracture Investigation", Ph.D. Dissertation, Univ. of Utah, Salt Lake City, 1970.
7. G. P. Anderson, S. J. Bennett and K. L. DeVries, Analysis and Testing of Adhesive Bonds, Academic Press, New York, 1977.
8. A. N. Gent, L. H. Lewandowski, "Blow-Off Pressures for Adhering Layers", J of Applied Polymer Science, 33, 1987, pp.1567-1577.
9. M. G. Allen and S. D. Senturia, "Microfabricated Structures for the Measurement of Adhesion and Mechanical Properties of Polymer Film", Proc of the American Chemical Society Division of Polymer Materials: Science and Engineering, 56, 1987, pp. 735-739.
10. M. G. Allen and S. D. Senturia, "Analysis of Critical Debonding Pressures of Stressed Thin films in the Blister Test", J of Adhesion, in press.
11. W G Knauss, "Delayed Failure - The Griffith Problem for Linearly Viscoelastic Materials", Int J Fracture Mech, 6 (1), 1970, pp 7-20.

- 12 M L Williams, "Initiation and Growth of Viscoelastic Fracture", Int. J. of Fracture Mechanics, 1, 1965, pp 292-310.
- 13 W S Blackburn, "Steady Crack Growth in a Linear Viscoelastic Material", Int J Fracture Mech, 7, 1971, pp 354-356.
- 14 M F Kanninen, "An Analysis of Dynamic Crack Propagation and Arrest for a Material Having a Crack Speed Dependent Fracture Toughness", Prospects of Fracture Mechanics, (Ed.) G C Sih, H C van Elst, D Broek, Noordhoff, 1974.
15. A. N. Gent and S. Kaang, "Pull-Off Forces for Adhesive Tapes", J of Applied Polymer Science, 32, (1986), pp.4689-4700.
- 16 M J Napolitano, A Chudnovsky, and A Moet, "The Constrained Blister Test: A New Approach to Interfacial Adhesion Measurements", Proceedings of the American Chemical Society, Division of Polymer Material Science and Engineering, 57, 1987, pp 755-759.
17. R.E. Smelser, "Evaluation of Stress Intensity Factors for Bimaterial Bodies Using Numerical Crack Flank Displacement Data", Int. J. Fracture, 15, 1979, pp.135-143.
18. R.E. Smelser, "On the J-Integral for Bi-Material Bodies", Int. J. Fracture, 13, 1977, pp.382-384.
19. S. Timoshenko and S Woinowsky-Krieger, Theory of Plates and Shells, McGraw Hill, New York, 1959.
20. R. Szilard, Theory and analysis of plates, Prentice-Hall, Englewood Cliffs, NJ 1974.
21. IMSL, The International Mathematics Subroutine Library, IMSL, INC, 1987.
22. O. C. Zienkiewicz, M. Watson and I. P. King, "A Numerical Method of Visco-Elastic Stress Analysis", Int J Mechanics and Science, 10, 1968, pp. 807-827.

## APPENDIX

### SIMULATION OF THE DEBONDING PROCESS FOR A STRIP OF VISCOELASTIC ADHESIVE TAPE

In Chapter 2, the test results of an adhesive tape with vinyl backing show that the debonding rate decreases as the debond radius increases. It is believed that this behavior is due to significant time dependent properties of the tape. A preliminary study to use a viscoelastic numerical solution to simulate the debonding process is attempted and discussed in this appendix.

The work has combined a general method of numerical viscoelastic stress analysis proposed by Zienkiewicz [22] and an energy formulation including the work of viscous dissipation, fracture initiation and growth in linearly viscoelastic material proposed by Williams [12]. By using the Zienkiewicz's method, the difficulty of retaining the stress history in the computer solution is avoided. With Williams' energy balance equation, the debonding rate can be determined. Thus, the simulation of the viscoelastic debonding process of the constrained blister test is possible.

For simplicity, several assumptions are made for the current model:  
1) the model is membrane stress dominated, and the bending effects are

negligible, 2) the debonding front is assumed to be straight, which is the case of constrained blister specimen with very large debond radius or a strip of specimen pressurized at the debonding area and constrained its deformation at the top, 3) the strain energy release rate is assumed to be constant, which is a material property, 4) the viscoelastic material is assumed to be a three parameter solid with the material properties,  $E_0$ ,  $E_1$ , and  $\mu_1$ , 5) perfect slipping between the specimen and the constraint.

Under the above assumptions, the profile of the pressurized specimen is shown in Fig. A-1. Since there is no localized (concentrated) force at the departure point between the suspended and contact region, we conclude from the zero resultant force in the vertical direction that the departure must be smooth, i.e., the slope is zero. Thus, it is easy to show the radius of curvature of the suspended region,  $\rho$ , is:

$$\rho = \frac{1}{2h} [h^2 + (a-b)^2] \quad (A-1)$$

where

$\rho$  is the radius of the curvature of the suspended region,

$h$  is the constraint height,

$a$  is half of the debond length,  $b$  is half of the length of the contact region.

Also, the membrane stress and the total length of the stretched

membrane from the center to the debond front are given as:

$$\sigma = \frac{p \rho}{t} \quad (\text{A-2})$$

$$\int_0^a (1 + \epsilon_x) dx = b + \frac{1}{2h} \left[ h^2 + (a-b)^2 \right] \cos^{-1} \left[ 1 - \frac{2h^2}{h^2 + (a-b)^2} \right] \quad (\text{A-3})$$

where

$\sigma$  is the membrane stress in the specimen,

$\epsilon_x$  is the membrane strain of the membrane in the x direction,

p is the applied pressure,

t is the thickness of the specimen.

Based on Zienkiewicz's method and Williams' energy balance equation, a computer program was written and the algorithm is listed in the following steps.

STEP 1. Input the necessary parameters for geometry, material properties, and load, which are h, t,  $E_0$ ,  $E_1$ ,  $\mu_1$ , and p. Assume an initial debond radius,  $a_0$ .

STEP 2. At time  $t=t_i$  ( $i=0,1,2,\dots$ ), check the total length of the specimen from the center to the debond front, and iterate Eq. (A-3) to convergence to determine the unknown quantity,  $b_i$ . In the program, the Newton-Raphson method is used for iteration.

$$b_1 + \frac{1}{2h} \left[ h^2 + (a-b_1)^2 \right] \cos^{-1} \left[ 1 - \frac{2h^2}{h^2 + (a-b_1)^2} \right] - \sum_{j=1}^i (1 + \epsilon_{x1}^j) \Delta a_j = 0 \quad (\text{A-4})$$

where

$$\epsilon_{x1}^j = \epsilon_{E1} + \epsilon_{c1}^j$$

$$\epsilon_{E1} = \frac{p}{2tE_0h} [h^2 + (a-b_1)^2].$$

$\epsilon_{c1}^j$  is the creep strain which is given in STEP 4. It should be noted that at  $t=0$ , the creep strain  $\epsilon_{c1}^j$  is zero and  $2b_0$  is the initial contact length.

STEP 3. Determine  $\rho_1$  and  $\sigma_1$  using Eqs.(A-1) and (A-2). Assume stress remains constant over next time increment,  $\Delta t$ .

STEP 4. Given a time increment,  $\Delta t_1$ , determine the creep strain:

$$\epsilon_{c1}^j = \frac{\Delta t_1}{\mu_1} \sigma_1 \quad \text{for } i=0$$

$$\epsilon_{c1}^j = \frac{\Delta t_1}{\mu_1} \sigma_1 + \left( 1 - \frac{E_1}{\mu_1} \Delta t_1 \right) \epsilon_{c1-1}^j \quad \text{for } i>0$$

where the superscript  $j$  denotes the position of the  $j$ th element,  $\Delta a_j$ .

STEP 5. Apply the energy power balance equation, Eq. (A-5), and

iterate to convergence to obtain the new debond radius,  $a_{i+1}$ , by the Newton-Raphson method.

$$\dot{I} - \dot{F} - D - \dot{E} = 0 \quad (\text{A-5-a})$$

where

$\dot{I}$  is the power input of the applied loading at the boundary,

$\dot{F}$  is the rate of increase of the strain energy,

$D$  is the viscoelastic dissipation,

$\dot{E}$  is the rate of increase of the surface energy.

$\dot{I}$ ,  $\dot{F}$ ,  $D$ , and  $\dot{E}$  for the current model are all per unit length and are given as :

$$\begin{aligned} \dot{I} &= p \dot{V} \\ &= p \frac{1}{\Delta t_1} \left[ \left[ h b_{i+1} + \frac{\rho_{i+1}^2}{2} \cos^{-1} \left( 1 - \frac{h}{\rho_{i+1}} \right) - \frac{1}{2} (\rho_{i+1} - h)(a_{i+1} - b_{i+1}) \right] \right. \\ &\quad \left. - \left[ h b_i + \frac{\rho_i^2}{2} \cos^{-1} \left( 1 - \frac{h}{\rho_i} \right) - \frac{1}{2} (\rho_i - h)(a_i - b_i) \right] \right] \quad (\text{A-5-b}) \end{aligned}$$

$$\begin{aligned} \dot{F} &= \frac{d}{dt} \int_{\text{vol}} \frac{1}{2} \sigma \epsilon_E d(\text{vol}) \\ &= \frac{p^2}{2E_0 t} \frac{1}{\Delta t_1} \left[ \rho_{i+1}^2 a_{i+1} - \rho_i^2 a_i \right] \quad (\text{A-5-c}) \end{aligned}$$

$$D = \int_{\text{vol}} \sigma \dot{\epsilon}_c d(\text{vol})$$

$$= \frac{p^2 \rho_{i+1}^2}{\mu_1 t} a_{i+1} - \frac{p \rho_{i+1} E_1}{\mu_1} \sum_{j=0}^i \varepsilon_{c1}^j \Delta a_j \quad (\text{A-5-d})$$

$$\begin{aligned} \dot{E} &= \frac{d}{dt} \int_s \gamma d(s) \\ &= \gamma \frac{a_{i+1} - a_i}{\Delta t_i} \end{aligned} \quad (\text{A-5-e})$$

where  $\gamma$  is the adhesive fracture energy which is assumed to be a constant material property.

STEP 6. Determine the debond rate,  $\dot{a}$ :

$$\dot{a} = \frac{a_{i+1} - a_i}{\Delta t_i} \quad (\text{A-6})$$

STEP 7. Repeat STEPS 2-6 to obtain the subsequent debonding radii and debond rates and thus simulate the debond process.

### Results and Discussions

From Figs. A-2 to A-6, the debonding process of the vinyl tapes is simulated and discussed in the following sections.

By modeling a vinyl tape as a three parameter solid, the debonding rates of the tape for different values of viscosity is simulated and

plotted versus time in Fig. A-2. For the vinyl tape tested in Chapter 2, the material constants are  $E_0 = 16.58$  MPa,  $E_1 = 35$  MPa, and  $\mu_1 = 8100$  MPa-sec, which are obtained by fitting the creep curve in Fig. 4. In the current discussion, the viscosity varies from 2000 MPa-sec to 20000 MPa-sec. The pressure,  $p$ , is 28.3kPa and  $h$ ,  $t$ , and initial debond radius are 3.175mm, 0.18mm, and 50mm, respectively. The adhesive fracture energy is assumed to be  $100 \text{ J/m}^2$  which is the value shown in Fig. 7. It is seen that for all cases, the debonding rates decrease as debond grows. For the curves with larger values of viscosity, the slopes of the debonding rate are smaller than the curves with smaller values of viscosity. Because as viscosity increases, material is more "elastic" within the chosen time span, thus, the results confirm the observations in Chapter 2 that the debonding rates of polyester tape which has little time dependent properties are nearly constant, while those of the vinyl tape decrease as the debond grows.

Figure A-3 illustrates the debonding rate versus time for different values of adhesive fracture energy. The parameters of material properties, geometry and loading conditions are the same as those in Fig. A-2. A decrease in debonding rates is also seen for all cases. It is seen that the debonding rate decreases as adhesive fracture energy increases. This phenomenon is reasonable because debond grows more slowly for a "tougher" bond. It is also seen that the values of the debonding rates in this simulation are 1-3 orders smaller than the

actual test data which were obtained from finite debond radii. Although the results suggest that if the debond radius is very large, the debond would be very slow, whether the magnitude of the debond rates obtained from the simulation is realistic is questionable. Unfortunately, neither analytical nor test results are available for verification.

Figures A-4 to A-6 illustrate the rates of change of energy,  $\dot{I}$ ,  $\dot{F}$ ,  $\dot{D}$ , and  $\dot{E}$ , normalized with respect to  $\dot{I}$ , versus time for adhesive fracture energy of 100, 110, and 150 J/m<sup>2</sup>, respectively. By comparing those three figures, it is seen that as adhesive fracture energy increases, both viscoelastic dissipation and the change of strain energy increase but the change of surface energy decrease. It is also seen that the dissipated energy is supplied from both input work and membrane strain energy, which shows that the membrane specimen is relaxing and doing work into the system. It should be noted that if the system is not perfectly free to slip between the specimen and constraint, the available strain energy would be much smaller. For the system with larger adhesive fracture energy, the viscoelastic dissipation is larger, which thus results in smaller debonding rate.

### Conclusions

A preliminary study to simulate the debonding process of a strip of viscoelastic adhesive tape subjected to constant pressure in the

debonding region was proposed in this appendix. The simulation was made possible by combining a numerical method of viscoelastic stress analysis and an energy formalism for viscoelastic material. The numerical results confirmed the observation in the CBT test that debonding rate decreases as the debond grows for the material with significant time dependent properties. The results also show that the debonding rate decreases as the adhesive fracture energy increases. Although the magnitude of the debonding rates obtained from the simulation waits for further verification, the preliminary results of the simulation suggest that the method is potentially useful for studying the viscoelastic fracture behavior for the adhesive systems.

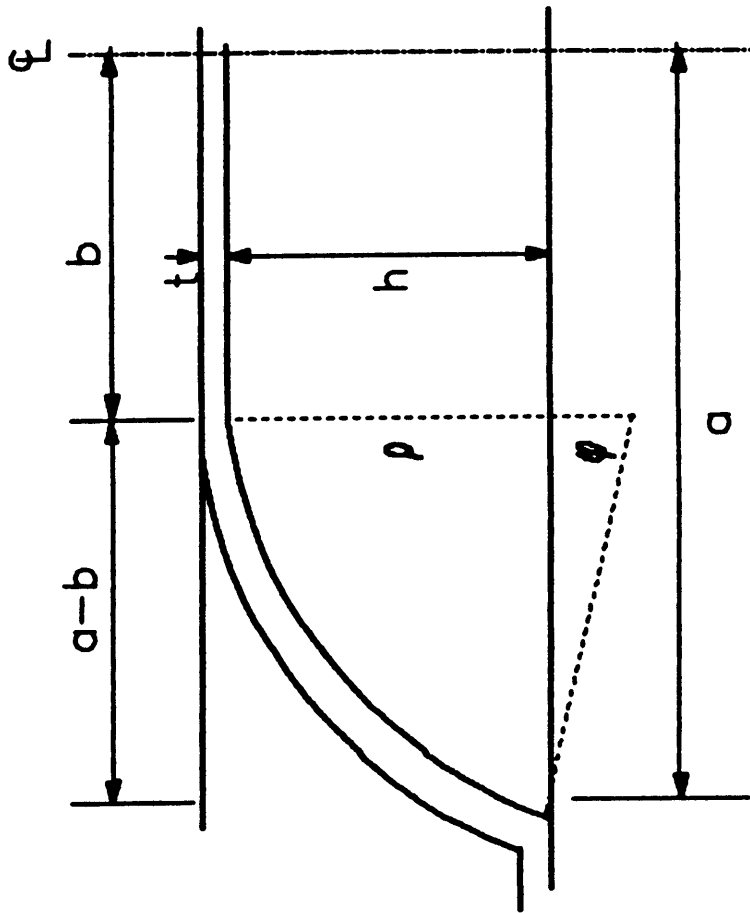


Figure A-1. The profile of a pressurized adhesive tape.

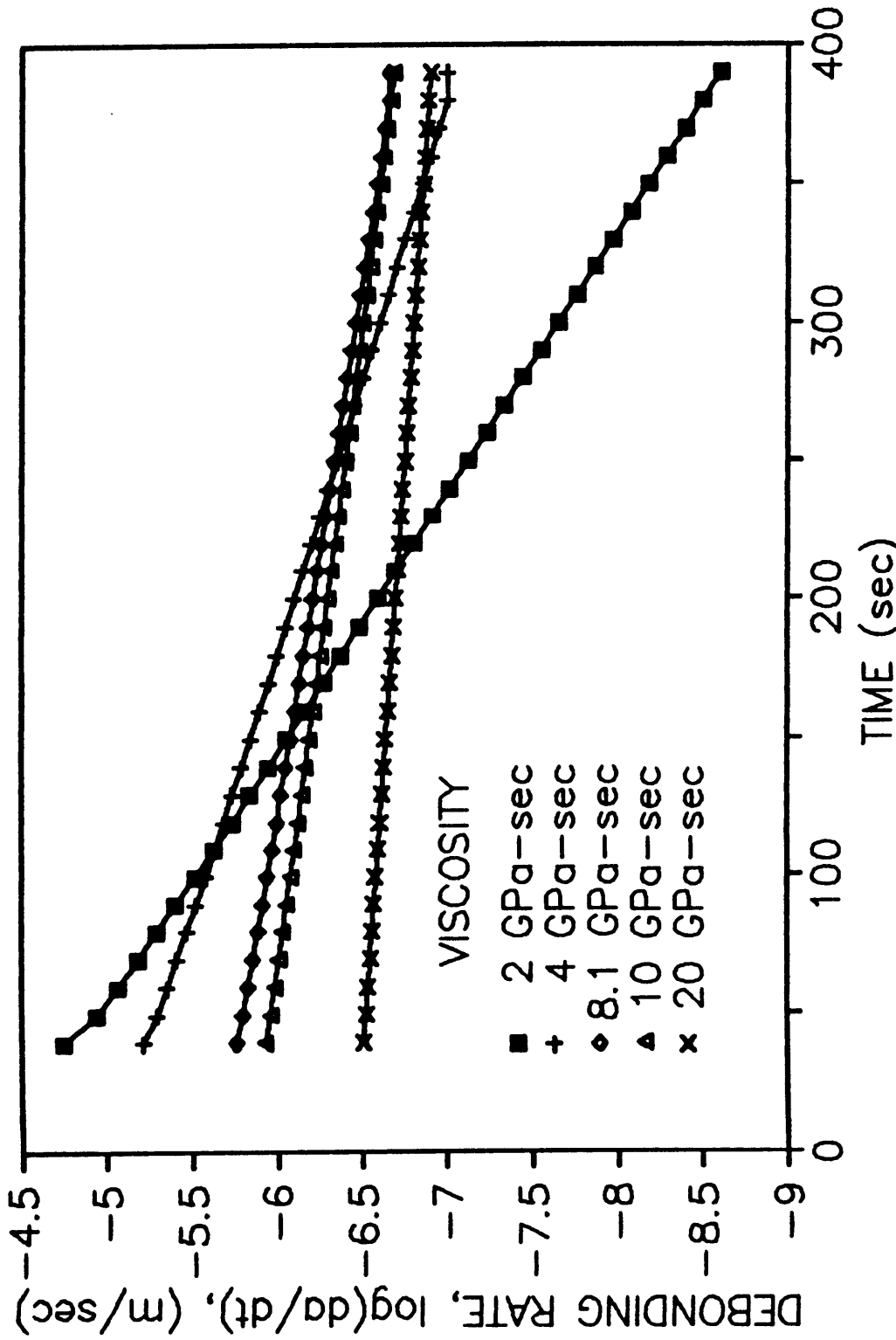


Figure A-2. Debond rate versus time for different values of viscosity.

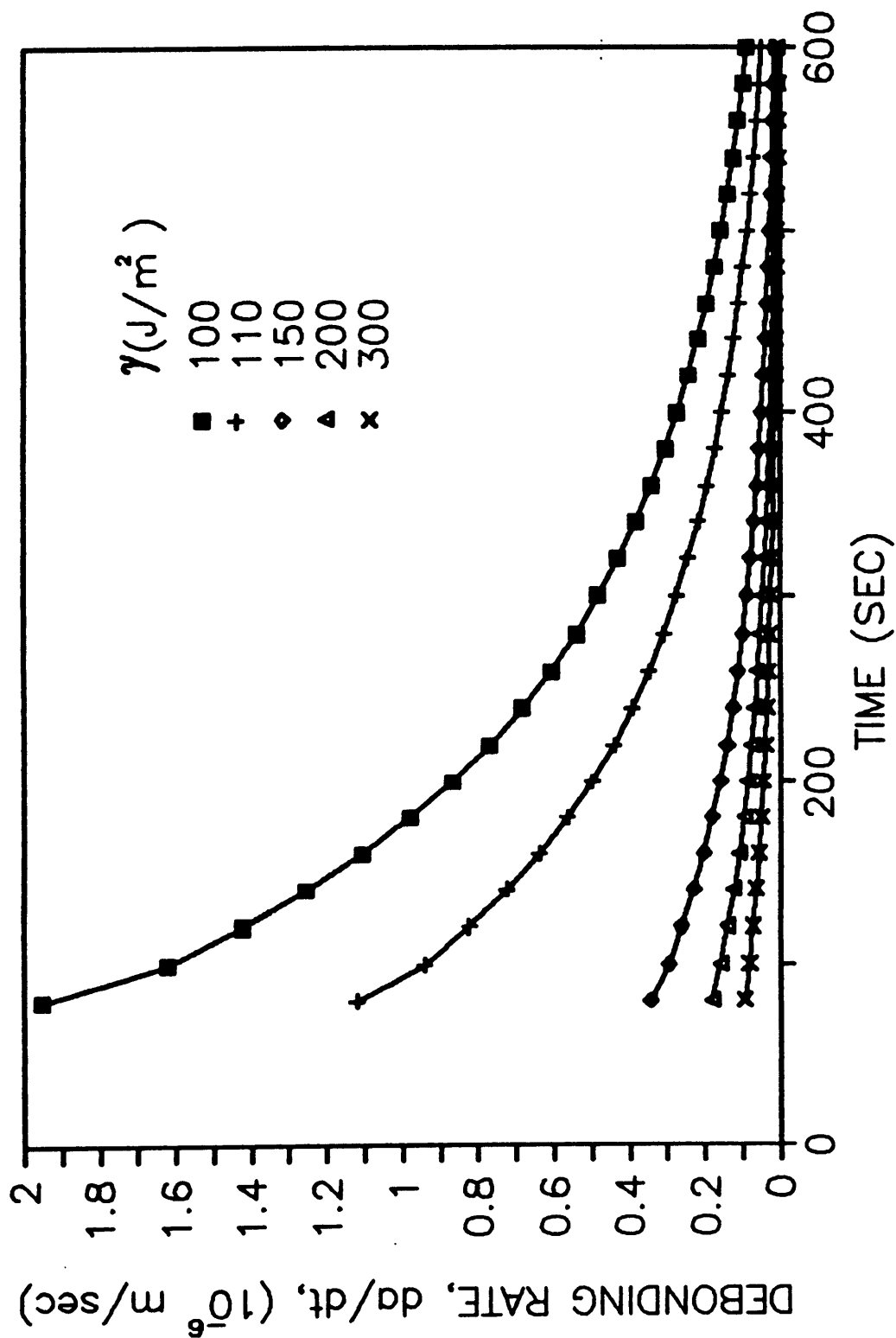


Figure A-3. Debonding rate versus time for different adhesive fracture energy.

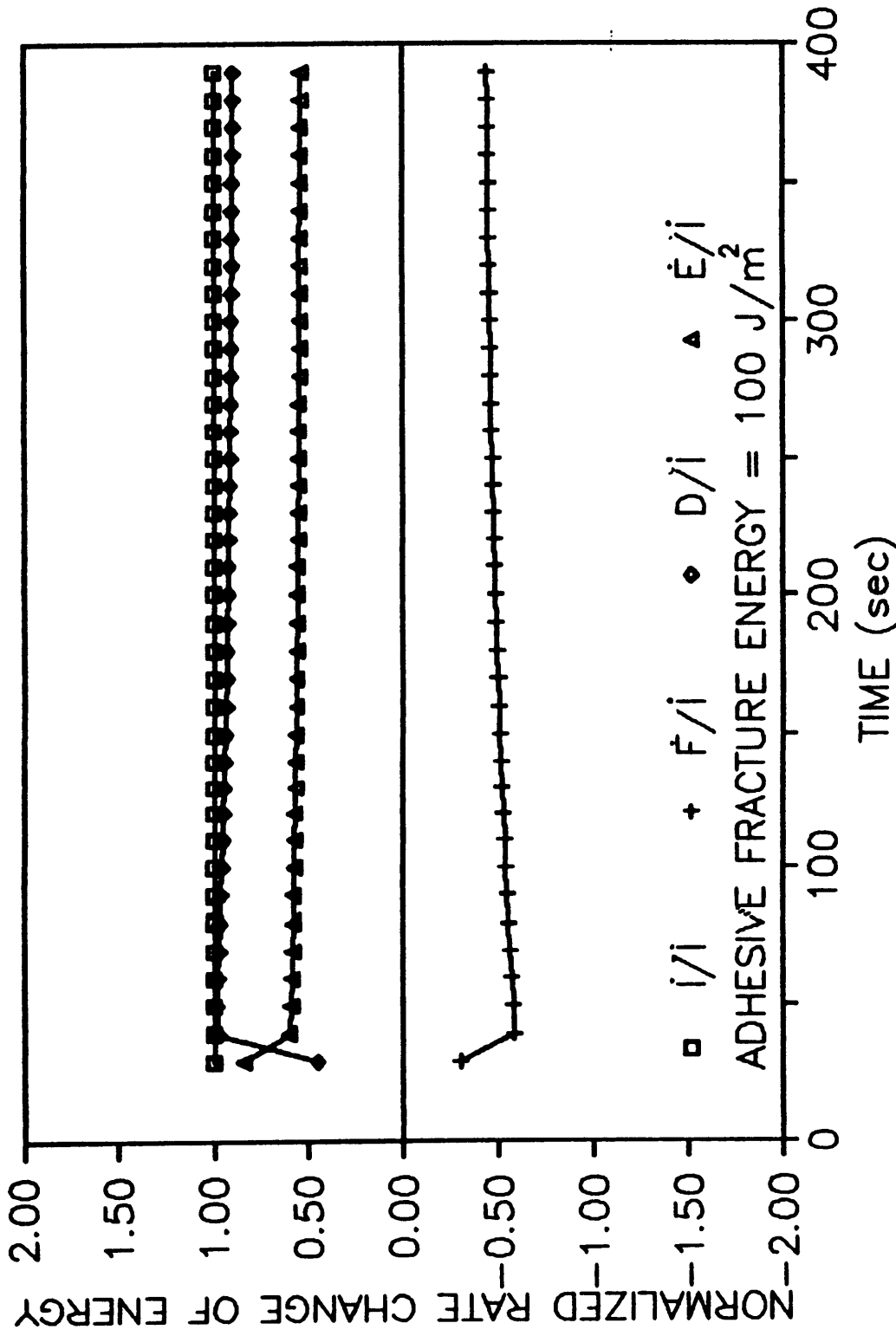


Figure A-4. Normalized rate of change of energy versus time for adhesive fracture energy equal to 100 J/m<sup>2</sup>

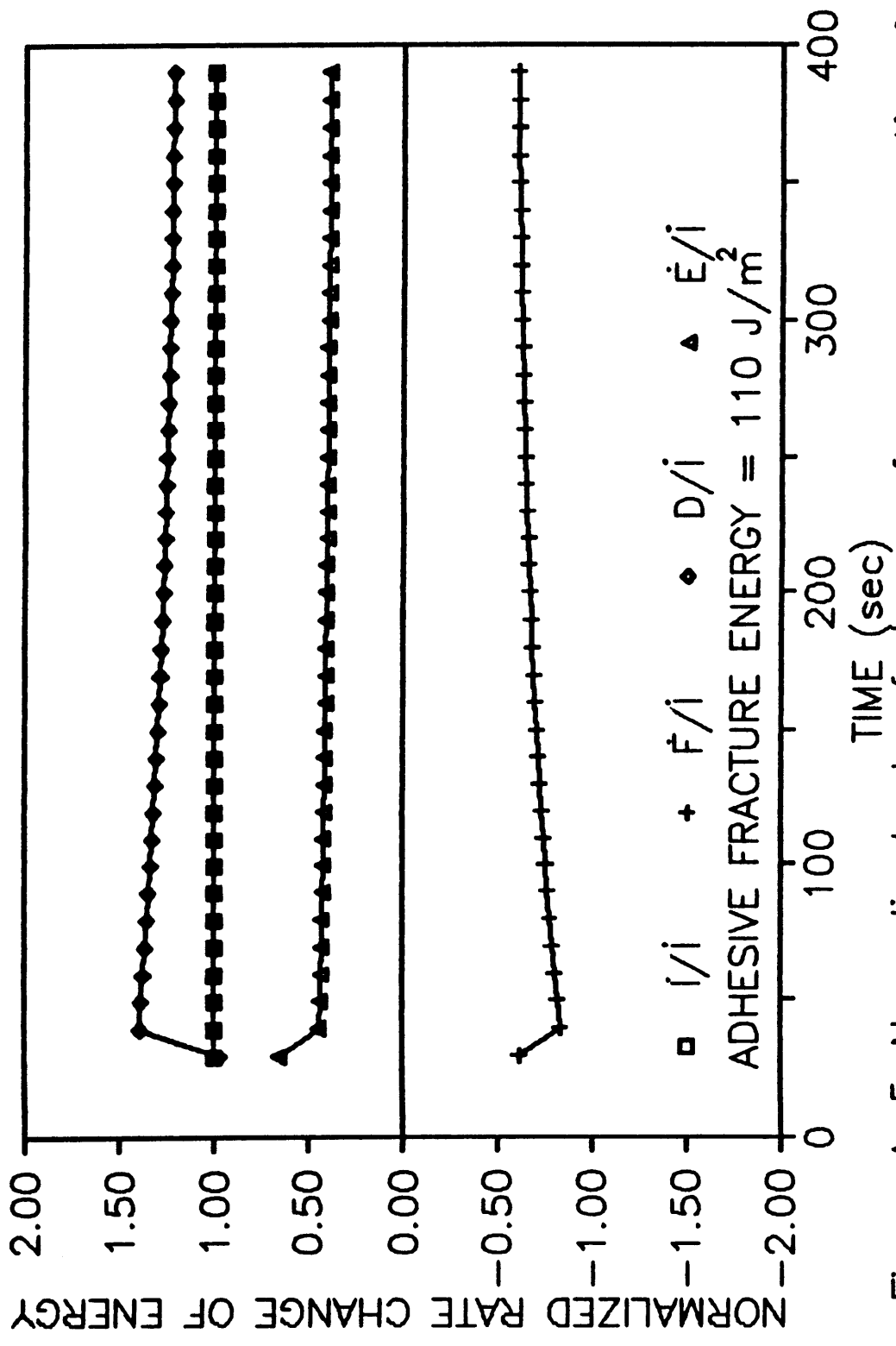


Figure A-5. Normalized rate of change of energy versus time for adhesive fracture energy equal to 110 J/m<sup>2</sup>

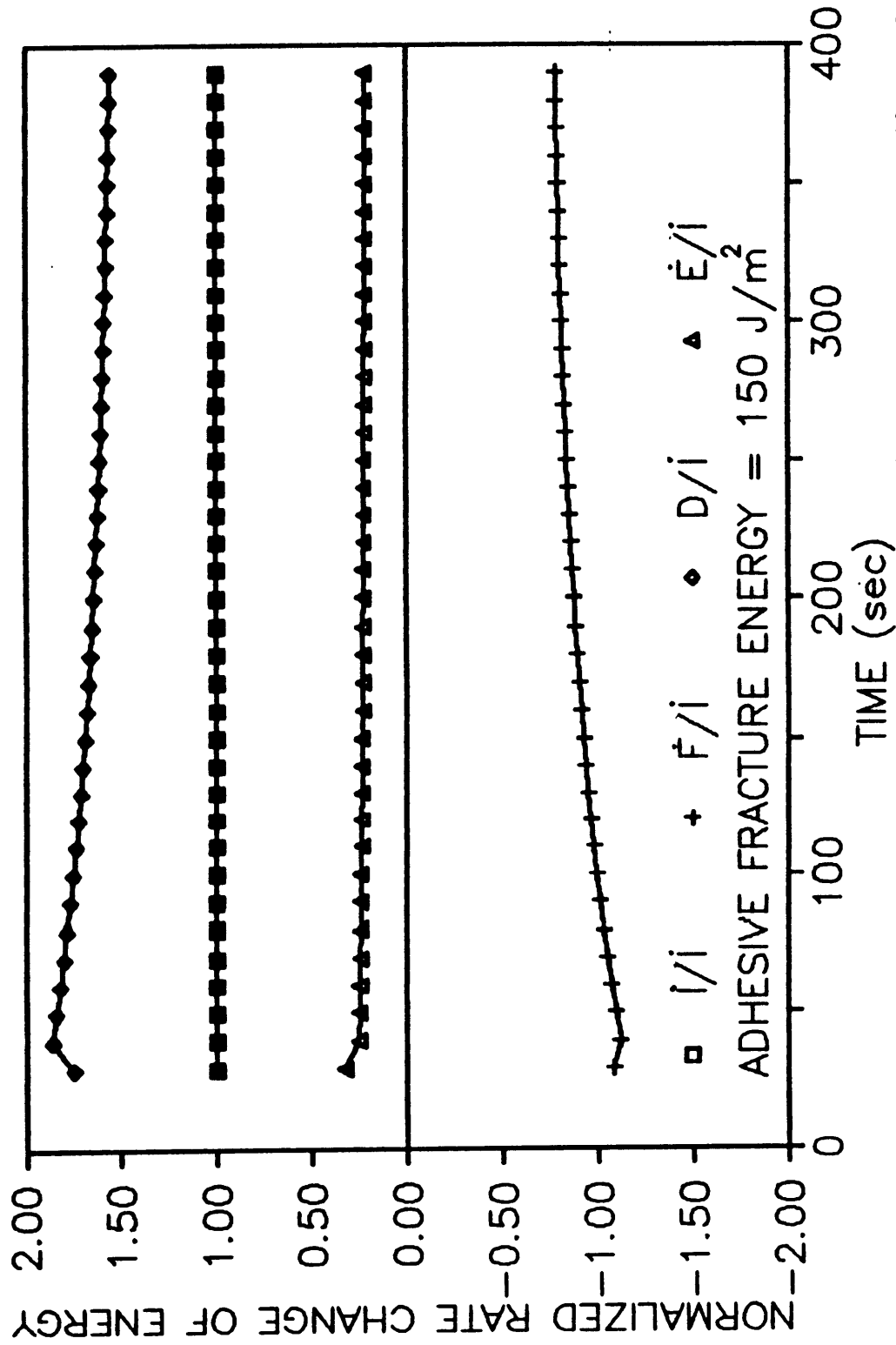


Figure A-6. Normalized rate of change of energy versus time for adhesive fracture energy equal to 150 J/m<sup>2</sup>

**The vita has been removed from  
the scanned document**